

1 **Towards understanding the variability in biospheric**
2 **CO₂ fluxes: using FTIR spectrometry and a chemical**
3 **transport model to investigate the sources and sinks of**
4 **carbonyl sulfide and its link to CO₂**

5
6 **Y. Wang¹, N. M. Deutscher^{1,2}, M. Palm¹, T. Warneke¹, J. Notholt¹, I. Baker³, J. Berry⁴,**
7 **P. Suntharalingam⁵, N. Jones², E. Mahieu⁶, B. Lejeune⁶, J. Hannigan⁷, S. Conway⁸,**
8 **J. Mendonca⁸, K. Strong⁸, J. E. Campbell⁹, A. Wolf¹⁰, and S. Kremser¹¹**

9 [1] Institute of Environmental Physics, University of Bremen, Bremen, Germany

10 [2] Centre for Atmospheric Chemistry, School of Chemistry, University of Wollongong,
11 Wollongong, Australia

12 [3] Colorado State University, Fort Collins, CO, USA

13 [4] Carnegie Institute of Washington, Stanford, CA, USA

14 [5] University of East Anglia, Norwich, UK

15 [6] Institute of Astrophysics and Geophysics, University of Liège, Liège, Belgium

16 [7] National Center for Atmospheric Research, Boulder, CO, USA

17 [8] Department of Physics, University of Toronto, Toronto, Canada

18 [9] University of California, Merced, CA, USA

19 [10] Princeton University, Princeton, NJ, USA

20 [11] Bodeker Scientific, Alexandra, New Zealand

21 Correspondence to: Y. Wang (w_yuting@iup.physik.uni-bremen.de)

22

23 **Abstract**

24 Understanding carbon dioxide (CO₂) biospheric processes is of great importance because the
25 terrestrial exchange drives the seasonal and inter-annual variability of CO₂ in the atmosphere.

1 Atmospheric inversions based on CO₂ concentration measurements alone can only determine net
2 biosphere fluxes, but not differentiate between photosynthesis (uptake) and respiration
3 (production). Carbonyl sulfide (OCS) could provide an important additional constraint: it is also
4 taken up by plants during photosynthesis but not emitted during respiration, and therefore is a
5 potential means to differentiate between these processes. Solar absorption Fourier Transform
6 InfraRed (FTIR) spectrometry allows for the retrievals of the atmospheric concentrations of both
7 CO₂ and OCS from measured solar absorption spectra. Here, we investigate co-located and quasi-
8 simultaneous FTIR measurements of OCS and CO₂ performed at five selected sites located in the
9 Northern Hemisphere. These measurements are compared to simulations of OCS and CO₂ using a
10 chemical transport model (GEOS-Chem). The OCS simulations are driven by different land
11 biospheric fluxes to reproduce the seasonality of the measurements. Increasing the plant uptake
12 of Kettle et al. (2002a) by a factor of three resulted in the best comparison with FTIR
13 measurements. However, there are still discrepancies in the latitudinal distribution when
14 comparing with HIPPO (HIAPER Pole-to-Pole Observations) data spanning both hemispheres.
15 The coupled biospheric fluxes of OCS and CO₂ from the simple biosphere model (SiB) are used
16 in the study. The CO₂ simulation with SiB fluxes agrees with the measurements well, while the
17 OCS simulation reproduced a weaker drawdown than FTIR measurements at selected sites, and a
18 smaller latitudinal gradient in the Northern Hemisphere during growing season. An offset in the
19 timing of the seasonal cycle minimum between SiB simulation and measurements is also seen.
20 Using OCS as a photosynthesis proxy can help to understand how the biospheric processes are
21 reproduced in models and to further understand the carbon cycle in the real world.

22

23 **1. Introduction**

24 Understanding the carbon dioxide (CO₂) biospheric processes within the carbon cycle is of great
25 importance, because: (1) the land carbon sink absorbs more than a quarter of the CO₂ emissions
26 released by human activities, which mitigates the increase of atmospheric CO₂ concentration; and
27 (2) terrestrial exchange drives CO₂ variability in the atmosphere on seasonal and inter-annual
28 time scales. The total biospheric CO₂ flux (net ecosystem production, NEP) is the sum of two
29 much larger terms with different seasonality and drivers: the carbon uptake of gross primary
30 production (GPP) and the release via respiration (Re). These fluxes are co-located, therefore,
31 typically only information about their sum (the NEP) is available when they are quantified. To

1 improve our knowledge of CO₂ biospheric processes, in particular how ecosystems will respond
2 to a changing climate, we would ideally like to understand the individual contributions of these
3 two fluxes.

4 Laboratory experiments (e.g. Goldan et al., 1988) have studied the pathway for carbonyl sulfide
5 (OCS) uptake by plants, which is similar to the uptake mechanism of CO₂ during photosynthesis.
6 Unlike CO₂, OCS uptake is a one-way process, and it is not emitted during respiration. Therefore
7 OCS could be used to differentiate between photosynthesis and respiration fluxes of CO₂
8 (Campbell et al., 2008). Flask measurements of OCS in the Northern Hemisphere show a clear
9 seasonal variation with a maximum in early spring and minimum in autumn, which is similar to
10 the seasonality of CO₂ (Montzka et al., 2007) as biospheric fluxes are the main driver of the
11 seasonal cycles for both species (Kettle et al., 2002a).

12 However, our knowledge about the sources and sinks of OCS remains limited. The estimates for
13 the global budget still have significant uncertainties. This makes it difficult to use OCS as a
14 photosynthetic tracer. The identified OCS sources include ocean emissions (direct emission and
15 indirect emission via oxidation of carbon disulfide (CS₂) and dimethyl sulfide (DMS)),
16 anthropogenic releases (direct emission and indirect emission via oxidation of CS₂), biomass
17 burning, and volcanoes. The sinks are plant uptake, soil uptake, reaction with hydroxyl radicals
18 (OH), reaction with oxygen atoms (O), and photolysis in the stratosphere. The ocean is believed
19 to be the most important source of OCS via both direct and indirect fluxes, and makes the biggest
20 contribution to the seasonality of OCS in the Southern Hemisphere (Kettle et al., 2002a). Plant
21 uptake is commonly recognized as the main sink of OCS, and is the dominant driver of seasonal
22 variation in the Northern Hemisphere (Goldan et al., 1988). Kettle et al. (2002a) analyzed OCS
23 monthly fluxes, and then calculated the global annual sources and sinks, which are in balance
24 within uncertainties. More recent studies (Suntharalingam et al., 2008; Berry et al., 2013)
25 indicated that the plant uptake in Kettle's estimation is too small, and therefore a corresponding
26 increase in sources is necessary to maintain the annual balance in the OCS budget. New studies
27 have also shown that the ocean and anthropogenic sources of OCS have been underestimated
28 (Guo et al., 2010; Berry et al., 2013; Campbell et al., 2015; Cheng et al., 2015; Launois et al.,
29 2015a) in Kettle et al. (2002a). The disagreement between measurements and simulations of OCS
30 indicated that the missing sources are mainly in the tropical region (Berry et al. 2013).
31 Anthropogenic emissions are unlikely to be the main reason for missing sources in that region,

1 and therefore ocean sources are likely to be responsible. Indeed, the ocean fluxes have large
2 uncertainties. The direct ocean flux has large temporal and spatial variations, and under certain
3 conditions could also act as a sink for OCS (Xu et al., 2001). Seawater measurements in some
4 regions of the ocean suggested that the open ocean could be a small source of OCS (Weiss et al.,
5 1995; Xu et al., 2001), and that indirect ocean emissions may play more important roles. Launois
6 et al. (2015a) calculated the direct ocean emissions using an ocean general circulation and
7 biogeochemistry model, and estimated a source of about 813 Gg S year⁻¹. In addition, OCS soil
8 uptake still has large uncertainties. Some soil types act as a source (Whelan et al., 2013) or only a
9 small sink (Xu et al., 2002; Steinbacher et al., 2004); however, the overall role of soils is as a sink
10 of OCS, with very different uptake rates between soil types and other physical parameters (Van
11 Diest and Kesselmeier, 2008; Sun et al., 2015). Another method to calculate the soil uptake is to
12 use the similarity of deposition to soils between molecular hydrogen (H₂) and OCS (Belviso et al.,
13 2013; H. Chen, private communication). This estimation yields a sink of about 500 Gg S year⁻¹,
14 largely dependent on the H₂ spatial distribution (Launois et al., 2015b). Therefore, improving the
15 estimation of the OCS sources and sinks is important when using it to investigate the biospheric
16 fluxes of CO₂. To achieve this aim, more OCS measurements at different latitudes and ecosystem
17 regions are needed to validate the estimates.

18 Until now, the measurements used for OCS studies are sparse. The typical measurements
19 involved, such as the NOAA/ESRL/GMD network, include ground-based and aircraft flask
20 sampling data. These ground-based in-situ measurements are only at limited sites and aircraft
21 measurements cover relatively short time periods. The emerging of the remote sensing data,
22 including ground-based (Notholt et al., 2003) and satellite (Barkley et al., 2008; Kuai et al., 2014;
23 Kuai et al., 2015; Glatthor et al., 2015) measurements, will potentially increase the number of
24 OCS measurements largely. The satellite data provide a wide distribution of OCS; however, they
25 are mainly sensitive in the upper troposphere and stratosphere (Barkley et al., 2008; Glatthor et
26 al., 2015) or mid troposphere (Kuai et al., 2014), and therefore have little help on constraining the
27 land fluxes. Ground-based solar absorption Fourier Transform InfraRed (FTIR) spectrometry
28 measures the absorption of both CO₂ and OCS. This can be used to retrieve the total and/or
29 partial atmospheric columns of these two gases. Compared to satellite retrievals, ground-based
30 FTIR OCS retrievals are also sensitive to low altitude and can therefore more directly capture the
31 variations due to the biospheric processes.

1 There are two networks of ground-based Fourier Transform InfraRed Spectrometers, both
2 recording high resolution solar absorption spectra: the Total Carbon Column Observing Network
3 (TCCON) (<http://www.tcon.caltech.edu>; Wunch et al., 2011), concentrating on CO₂ and
4 methane in the near-infrared (NIR); and the Network for the Detection of Atmospheric
5 Composition Change InfraRed Working Group (NDACC-IRWG), measuring spectra in the mid-
6 infrared (MIR). CO₂ total columns are retrieved from NIR spectra, while OCS profiles and
7 columns can be calculated from MIR spectra using dedicated software packages. CO₂ could also
8 be retrieved from MIR spectra, but the retrieval sensitivity dominates in the stratosphere, and
9 therefore the CO₂ seasonal cycle cannot be well captured (Barthlott et al., 2015; Buschmann et al.,
10 2015). We will only use TCCON CO₂ product in this study. The NDACC-IRWG sites provide a
11 potential database of OCS, that could be used to assess its sources and sinks. Kettle et al. (2002b)
12 used FTIR OCS total column measurements to estimate hemisphere-integrated OCS flux and
13 confirmed their understanding of OCS global budget. However, the measurements could not put
14 constraints on the relative magnitude of vegetative uptake and ocean-related emissions. B.
15 Lejeune (private communication) has improved the OCS retrieval, with a better accuracy on
16 seasonal amplitude, which is important for studying the carbon cycle and resolving temporal
17 variability of OCS fluxes. Additionally, some sites measure in both NIR and MIR spectral
18 regions, and therefore provide co-located and quasi-simultaneous CO₂ and OCS measurements.

19 The aim of this work is to exploit ground-based FTIR measurements of OCS to evaluate its
20 sources and sinks, and further to use OCS as a tracer of photosynthesis. This is the first time
21 using total/partial column data from FTIR networks to study the relationship
22 between OCS and CO₂. When interpreted by models, total column measurements are much less
23 sensitive to assumptions on the boundary layer mixing, because every molecule in the
24 atmospheric column is detected, independent of whether it is at the surface or in the upper
25 troposphere. In order to obtain realistic fluxes by inverse models, assumptions must be made on
26 the vertical mixing in the atmosphere, which is currently a large uncertainty in the transport
27 of most models (Wunch et al., 2011; Yang et al., 2007; Keppel-Aleks et al., 2011). Therefore,
28 column measurements of OCS and CO₂ could provide additional information for evaluating their
29 terrestrial exchange.

30 In section 2, 3, and 4, we will describe the measurements, models, and inter-comparison between
31 FTIR and model, respectively. In sections 5, we first analyze the FTIR measurements of OCS and

1 CO₂ at selected sites. Then we compare OCS measurements to model simulations to evaluate the
2 sources and sinks of OCS. Finally, we will discuss what can be learnt about CO₂ biospheric
3 fluxes from OCS. The publication closes with the conclusion and outlook.

4

5 **2. Measurements**

6 **2.1 FTIR**

7 Five measurement sites are used in this study as a starting point for the research aim of using
8 OCS to differentiate between photosynthetic and respiration fluxes of CO₂ (see details in Table 1).
9 Ny-Ålesund and Bremen, which are operated by the University of Bremen, and Eureka, operated
10 by the Canadian Network for the Detection of Atmospheric Change (CANDAC) and the
11 University of Toronto, measure both OCS and CO₂. The Jungfraujoch and Mauna Loa, operated
12 by the University of Liège and National Center for Atmospheric Research, respectively, only
13 measure in the MIR spectral region, and therefore TCCON-type CO₂ data are not available.

14 OCS profiles and total columns were retrieved using the SFIT-4 algorithm, based on the optimal
15 estimation technique (Rodgers, 2000). A mixed spectroscopy based on the HITRAN 2012
16 database was used in the retrievals. The a priori profile of OCS was provided by G. Toon (private
17 communication), and modified according to the average tropopause height above each site
18 (constant in the troposphere, and decrease above tropopause). Four spectral micro-windows were
19 used in the fitting (B. Lejeune, private communication), containing the OCS v3 band P32, P28,
20 P25, and P18 lines, respectively. Before fitting, spectra with a signal-to-noise ratio (SNR) of less
21 than 100 were discarded. Post-fitting, retrievals with a root-mean-square (RMS) residual of
22 greater than 0.5% were excluded before subsequent analysis. The retrieval parameters are
23 summarized in Table 2.

24 To minimize the influence of the variations in stratosphere, the tropospheric partial columns were
25 calculated from the surface to 9.8 km, based on the structure of the averaging kernels. In total,
26 approximately 2.5 degrees of freedom for signal (DOFS) for total columns were obtained for all
27 three sites. The DOFS for 0 to 9.8km is about 1. To make the values comparable to the in situ
28 measurements, the tropospheric OCS column-averaged dry-air mole fractions (xOCS) were
29 derived using Eq. (1):

1 $x_{\text{OCS}} = \text{Tropospheric OCS partial column} / \text{Tropospheric dry - air partial column}$ (1)

2 The uncertainties are calculated using contributions from measurement uncertainties (S_m), and
3 forward model parameter uncertainties (S_f) based on Rodgers (2000). The interference
4 uncertainties (S_{int}) are calculated as described by Rodgers and Connor (2003). The total
5 uncertainty in the tropospheric partial columns ($S_{\text{total_tropo}}$) was determined by adding these three
6 components at each tropospheric layer (i) in quadrature:

$$7 \quad S_{\text{total_tropo}} = \left(\sum_1^n (S_m(i)^2 + S_f(i)^2 + S_{\text{int}}(i)^2) \right)^{1/2} \quad (2)$$

8 The average uncertainties in the tropospheric partial columns from 2005 to 2012 are about 3% for
9 all the sites.

10 The OCS retrievals from the FTIR spectra are not calibrated to account for biases due to the
11 spectroscopy and other factors, therefore the means of the FTIR and in-situ measurements have
12 an offset.

13 We use the GGG2012 version of the TCCON CO_2 data, available on <http://tccon.ornl.gov/2012>.
14 CO_2 total columns as well as O_2 total columns were retrieved from near-infrared spectra using
15 GFIT, following the TCCON standard procedure (Wunch et al., 2011). The CO_2 column is
16 retrieved from two bands centered at 6228 cm^{-1} and 6348 cm^{-1} , while O_2 is retrieved from the
17 electronic band centered at 7882 cm^{-1} . CO_2 column-averaged dry-air mole fractions (DMF) were
18 calculated by the following equation:

$$19 \quad x_{\text{CO}_2} = \text{CO}_2 / \text{O}_2 \times 0.2095 \quad (3)$$

20 **2.2 HIPPO**

21 The HIPPO (HIAPER Pole-to-Pole Observations) study of carbon cycle and greenhouse gases
22 provides pole-to-pole measurements of meteorology, atmospheric chemistry, and aerosol content
23 over the Pacific Ocean. HIPPO flew five month-long missions between January 2009 and
24 September 2011 at different seasons. In this work, we use the NOAA flask sample data product
25 of HIPPO (Wofsy et al., 2012), which provides additional information on the latitudinal
26 distribution of the OCS and CO_2 . The OCS data (referred to as HIPPO-OCS) used in the work
27 were measured by the NOAA “Whole Air Sampler-Montzka Mass Spectrometer #2” (NWS-
28 M2), while CO_2 concentrations (referred to as HIPPO- CO_2) were measured by the NOAA
29 “Whole Air Sampler-Measurement of Atmospheric Gases that Influence Climate Change”

1 (NWAS-MAGICC).

2

3 **3. Model simulations**

4 **3.1 GEOS-Chem and CO₂ simulation**

5 The GEOS-Chem chemical transport model (version v9-01-03) is used in this study to simulate
6 the concentrations of CO₂ and OCS in the global atmosphere. It is driven by assimilated
7 meteorological observations from the Goddard Earth Observing System (GEOS) of the NASA
8 Global Modeling Assimilation Office (GMAO) (Bey et al., 2001). The simulations were run
9 using GEOS-5 meteorology from 2004 to 2012 on a horizontal grid resolution of 2 by 2.5 degrees
10 (latitude by longitude), with 47 vertical levels. Taking 2004 as one year spin-up, we analyze the
11 results from 2005 to 2012 based on hourly model output.

12 The CO₂ simulation module in GEOS-Chem was developed by Suntharalingam et al. (2003;
13 2004), and updated by Nassar et al. (2010). The CO₂ fluxes used in GEOS-Chem version v9-01-
14 03 include monthly fluxes of fossil fuel emissions from the Carbon Dioxide Information Analysis
15 Center (CDIAC) inventory; biomass burning from the Global Fire Emission Database (GFED3);
16 ocean exchange from Takahashi et al. (2009); and annual biofuel fluxes from Yevich and Logan
17 (2003). GEOS-Chem uses CO₂ biospheric fluxes calculated from the Carnegie-Ames-Stanford-
18 Approach (CASA; Olsen and Randerson, 2004) model for the year 2000 as a standard input, so
19 that the biospheric fluxes do not have inter-annual variability. The CASA biospheric fluxes are
20 balanced to zero at every grid, and therefore another terrestrial flux, which is referred to as the
21 residual annual terrestrial exchange, is added to the simulation (Baker et al., 2006). In this study,
22 we substitute the CASA biospheric fluxes with those calculated by the Simple Biosphere model
23 (SiB; detail in section 3.3).

24 **3.2 OCS simulation**

25 The OCS module is developed from the version of Suntharalingam et al. (2008), and added to
26 GEOS-Chem v9-01-03. It is largely based on the gridded flux inventories of Kettle et al. (2002a),
27 hereafter referred to as K2002. The input fluxes from K2002 include ocean emissions,
28 anthropogenic emissions, plant uptake, and soil uptake. The OCS biomass burning emission is
29 calculated from CO emissions (from GFED3) using a scale factor from Nguyen et al. (1995). The

1 tropospheric OH oxidation of OCS is calculated from OH monthly data (Park et al., 2004) and a
2 temperature dependent rate (Atkinson et al., 1997). In addition, we included stratospheric loss
3 (total loss from reaction with OH, O, and photolysis) in the OCS simulation to avoid the OCS
4 accumulation above the troposphere. This stratospheric loss is computed using the altitude
5 dependent loss rate from Chin and Davis (1995). The OCS simulation with K2002 provides a
6 baseline for evaluating the sources and sinks of OCS.

7 **3.3 The Simple Biosphere model (SiB)**

8 To study the relationship between OCS and CO₂, we used the coupled fluxes from SiB. SiB was
9 developed as a lower boundary for atmospheric models (Baker et al., 2013; Sellers et al., 1986),
10 and has been coupled to General Circulation Models (GCMs; Sato et al., 1989; Randall et al.,
11 1996) as well as mesoscale models (Denning et al., 2003; Nicholls et al., 2004; Wang et al., 2007;
12 Corbin et al., 2008). Berry et al. (2013) incorporated the calculation of OCS uptake through
13 stomata and in ground into SiB3 based on the biochemical mechanism for uptake of OCS by
14 leaves and soils. This version of SiB is called SiB3-COS, and provides coupled simulations of
15 CO₂ and OCS biospheric fluxes, including OCS plant uptake, OCS soil uptake, GPP, and CO₂
16 respiration. For this research, SiB3 simulations were performed on a 1.0 by 1.25 degree (latitude
17 by longitude) grid, with meteorology provided by the Modern-Era Retrospective analysis for
18 Research and Applications (MERRA; Reinecker et al., 2011). Precipitation fields were scaled to
19 match Global Precipitation Climatology Project (GPCP; Adler et al., 2003) amplitudes globally.
20 Respiration is scaled in SiB3, following Denning et al. (1996), to match productivity on a long-
21 term basis; individual years are not in exact balance. Phenology (LAI, fPAR) is determined
22 prognostically following Stöckli et al. (2008; 2011). Global GPP for the years 2000-2012
23 averages 120 Gt C year⁻¹, in reasonable agreement with flux tower-based estimates (Beer et al.,
24 2010; Jung et al., 2011), although the spatiotemporal distribution of carbon uptake and efflux is
25 uncertain.

26 In SiB, the OCS plant uptake is not scaled from GPP using a single factor, but estimated by
27 mechanistic parameterization, consisting of several steps (Berry et al., 2013). OCS first diffuses
28 from the boundary layer to the canopy, then from the canopy to the stomata, the stomata to the
29 cells, and then is consumed in the cells. In the first step, the diffusion amount depends on the
30 boundary layer concentration and diffusion conductance. The subsequent diffusion steps also

1 depend on the conductance. The diffusion pathway of OCS is the same as that of CO₂, but with
2 different conductance. The consumption of OCS in the cells is by the enzyme carbonic anhydrase
3 (CA), which is co-located with the enzyme that consumes CO₂ – Rubisco (Protoschill-Krebs and
4 Kesselmeier, 1992; Protoschill-Krebs et al., 1996). CA activity and mesophyll conductance are
5 suggested to be proportional to the V_{max} of Rubisco by some studies (Berry et al., 2013; Badger
6 and Price, 1994; Evans et al., 1994), and this relationship is used in SiB to simulate the OCS
7 uptake.

8 Soil uptake of OCS is a function of the activity of CA, as well as the condition of the soil (Berry
9 et al., 2013; Van Diest and Kesselmeier, 2008). Due to the lack of information on soil CA activity,
10 the soil uptake is instead calculated as a function of heterotrophic respiration (Rh), because
11 measurements show that the OCS soil uptake is proportional to Rh (Yi et al., 2007). In Berry et al.
12 (2013), the entire soil column was considered when scaling OCS soil uptake to Rh. Subsequent
13 model versions have modified this treatment to consider only the top 20 cm of soil. Additionally,
14 $J(\theta)$ (Equation 4, Berry et al., 2013) is no longer monotonically increasing from wet to dry soil,
15 but rather follows a function (as Rh does in SiB) that peaks at an ‘optimum’ soil wetness based
16 on soil character (Raich et al., 1991). Soil OCS uptake in SiB has been reduced from
17 approximately one-half to around one-quarter of the uptake rate of the canopy, which is more in
18 line with observations.

19 In this work, all the simulations were run using GEOS-Chem transport model. Two OCS land
20 fluxes were used, K2002 and SiB, in the OCS simulations, summarized in Table 3. In the analysis,
21 the simulations with different fluxes will be referred to as the fluxes names, as shown in Table 3.

22

23 **4 Comparison between FTIR retrievals and model**

24 When comparing FTIR data with model simulations, the a priori and vertical sensitivity of the
25 retrievals must be considered. We use the method described by Rodgers and Connor (2003). The
26 hourly model vertical profiles were selected at the nearest grid point to the measurement sites and
27 at measurement hours. The OCS profiles were smoothed by the FTIR a priori and averaging
28 kernels of each measurement following the equation.

$$29 \quad X_s = X_a + A(X_m - X_a) \quad (4)$$

30 where X_s , X_a and X_m are smoothed, a priori and model vertical profile, respectively, and A is the

1 averaging kernel matrix. The tropospheric xOCS was then calculated using Eq. (1).

2 For CO₂ column retrievals, Eq. (4) is modified (Wunch et al., 2010) to yield:

$$3 \quad C_s = C_a + h^T \times a^T \times (X_m - X_a) \quad (5)$$

4 where C_s and C_a are smoothed and a priori CO₂ column-averaged DMF, h describes the vertical
5 summation, a is the TCCON absorber-weighted column averaging kernel. TCCON averaging
6 kernels are largely dependent on the solar zenith angle. Here we use the standard TCCON
7 averaging kernel product, which provides the averaging kernels at five degree solar zenith angle
8 intervals. The averaging kernels used here are interpolated to the solar zenith angle at the time the
9 measurement was made.

10

11 **5 Results**

12 **5.1 The relationship between OCS and CO₂ in FTIR measurements**

13 Weekly mean calculated xCO₂ and xOCS are shown in Figure 1. Both CO₂ and OCS show clear
14 seasonal variation with a maximum in late winter or early spring and a minimum in autumn. At
15 Eureka, Ny-Ålesund and Bremen, OCS reaches its minimum about one month later than CO₂.
16 The drawdown of CO₂ results from the sum of the photosynthesis uptake and respiration
17 emission. When respiration exceeds photosynthesis, CO₂ starts increasing, while OCS is still
18 decreasing due to the contribution of photosynthesis.

19 The FTIR measurements show a relative seasonal amplitude of OCS of about six times that of
20 CO₂, which is similar to the ratio derived from in-situ measurements (Montzka et al., 2007). The
21 different magnitudes of the seasonal amplitudes are attributed to the absence of respiration, and to
22 the leaf-scale relative uptake (LRU) rate of OCS to CO₂. Some laboratory and field experiments
23 have shown that plants prefer OCS to CO₂, and obtained a LRU in the range of 1.3-5.5 for
24 different species (Sandoval-Soto et al., 2005; Seibt et al., 2010; Stimler et al., 2010; Xu et al.,
25 2002). If the LRU rate is known, the seasonal cycle of GPP can be determined from the OCS
26 seasonal cycle, and measurements of OCS can be used to quantify GPP.

27 The seasonal amplitudes of both CO₂ (approximately 3%) and OCS (approximately 18%) in Ny-
28 Ålesund and Eureka are bigger than those in Bremen (approximately 2% and 13% for CO₂ and
29 OCS, respectively), Jungfraujoch (approximately 10% for OCS) and Mauna Loa (approximately

1 9% for OCS). This is caused by the effect of the boreal forest combined with advective transport.
2 The photosynthesis in the boreal forest is strong during the polar day, leading to the rapid
3 drawdown of both CO₂ and OCS, which can be clearly seen in the measurements at the Arctic
4 sites. For Jungfraujoch, the seasonal amplitude is smaller than that in Bremen, which partly
5 results from its high altitude, so that the variation in the lower atmosphere is not captured.
6 Eliminating altitudes below 3.5km (the altitude of Jungfraujoch) from the calculation of xOCS at
7 Ny-Ålesund and Bremen decreases their seasonal cycle amplitude by approximately 10%.

8 **5.2 OCS sources and sinks implied from FTIR measurements and model** 9 **comparisons**

10 **5.2.1 Initial simulation of OCS**

11 Prior to using the model relationship between OCS and CO₂, we assess the accuracy of the OCS
12 fluxes, starting with fluxes of K2002, referred to as the initial simulation.

13 The simulations of OCS with K2002 are shown as orange plus signs in Figure 2. The initial
14 simulation (K2002) underestimates the seasonal amplitude, as reported by previous studies
15 (Suntharalingam et al., 2008; Berry et al., 2013). Plant uptake is thought to be the dominant
16 driver of seasonal variation in the Northern Hemisphere, so increasing the plant uptake should
17 increase the seasonal amplitude. K2002 used a model based on Net Primary Production (NPP) to
18 calculate the plant uptake of OCS, assuming the relative uptake rates for OCS and CO₂ were the
19 same (Kettle et al., 2002a). That is,

$$20 \text{ OCS uptake} = \text{NPP} \times [\text{OCS}]/[\text{CO}_2] \quad (6)$$

21 where [OCS] and [CO₂] are the atmospheric concentrations of OCS and CO₂, respectively. .
22 Considering that OCS is taken up by plants irreversibly, while CO₂ is also released through
23 respiration, and plants favor OCS over CO₂, a model based on GPP has been suggested to replace
24 the NPP-based model (Sandoval-Soto et al., 2005):

$$25 \text{ OCS uptake} = \text{GPP} \times [\text{OCS}]/[\text{CO}_2] \times \text{LRU} \quad (7)$$

26 GPP is about two times as large as NPP, and the global averaged LRU is in the range of 1.3 – 3.1
27 (Seibt et al., 2010; Stimler et al., 2012; Berkelhammer et al., 2014), so that in the GPP-based
28 model, the OCS plant uptake is increased by a factor of 2.6 to 6.2 from the NPP model. Therefore
29 the plant uptake in K2002 needs to be increased to match the seasonal cycle of the measurements.

1 Additionally, the simulation underestimates the mean OCS value at Mauna Loa, implying a
2 missing source at low latitudes. Berry et al. (2013) indicated that the missing source after
3 increasing the land sinks is likely from the ocean, and distributed mainly in the tropical region.

4 **5.2.2 Simulations with rescaled K2002 fluxes**

5 In order to improve the OCS simulation, we rescaled the OCS fluxes to find a better match to the
6 measurements. This scaling, while not optimal, provides an idea of the sensitivity of the
7 simulation to these processes. Following Suntharalingam et al. (2008) we modified the K2002
8 fluxes by increasing the plant uptake by factors of two (K2002x2, Figure 2. blue asterisks) and
9 three (K2002x3, Figure 2. green stars). To balance the global budget, the ocean emissions were
10 modified based on previous studies, which include increasing the ocean emissions in the tropical
11 region, and decreasing the ocean emissions in the Southern Ocean (Suntharalingam et al., 2008).
12 This will be further discussed in section 5.2.3. The details of the rescaled OCS sources and sinks
13 are shown in Table 3.

14 The simulations with rescaled fluxes increased the seasonal cycle amplitudes, and decreased the
15 peak and mean values at the high latitude sites. The seasonal amplitude of the simulation with
16 K2002x2 matches the measurements better than the original Kettle fluxes. K2002x3 further
17 increases the seasonal cycle amplitude. There is no inter-annual variability in the fluxes, so these
18 simulations cannot reproduce the yearly varying seasonal amplitudes. However, from the
19 averaged seasonal cycles (Figure 2, right panels), the simulations with K2002x3 match the
20 measurements better than K2002x2.

21 Mauna Loa is more affected by ocean fluxes than the other high latitude sites, indeed, on average,
22 the simulated OCS amounts at Mauna Loa did not change with the rescaling of the fluxes. This is
23 in contrast to the other sites, where the influence of the land sink dominates; at Mauna Loa, the
24 increased tropical ocean sources negate the effect of the increased land sink. The simulated
25 seasonal cycles show a peak in summer, which mainly results from the seasonality of the ocean
26 fluxes. This is different from the measurements: the maximum measured OCS abundance occurs
27 in spring, suggesting that the temporal variation of the ocean sources also needs to be adjusted.

28 **5.2.3 HIPPO latitudinal distribution**

29 To evaluate the latitudinal distribution of the rescaled fluxes, we compared the model simulations
30 with HIPPO-OCS (Figure 3). To facilitate this comparison, the model mean was adjusted (by

1 adding an offset of 30 ppt) to match the mean of the HIPPO measurements. The latitudinal
2 distribution of the simulation with K2002 poorly matches the HIPPO-OCS. The K2002
3 simulation results in OCS concentrations that are too low in the tropics and too high in the
4 Southern Hemisphere compared to the measurements from all five campaigns. In late northern
5 summer (HIPPO-5) and autumn (HIPPO-2), the model is higher than the measurements in the
6 boreal region, because the modeled plant uptake is too weak. After rescaling the plant uptake and
7 ocean emissions, the latitudinal distribution of the simulation shows better agreement with
8 HIPPO-OCS. In the Southern Hemisphere, the K2002x3 simulation has a higher value than
9 K2002x2, caused by the larger ocean emissions in the tropics. There are still mismatches,
10 especially in the tropical and northern temperate regions during HIPPO-2 and HIPPO-3, likely
11 because sources in this region are too low in the model. This is also seen in Mauna Loa
12 comparison between simulations and measurements. Increasing the ocean emissions in the
13 Northern Hemisphere by a factor of two (not shown) results in a simulated increase in OCS in
14 northern summer, at the time that ocean fluxes are greatest, while winter is hardly affected.
15 Simply rescaling the fluxes based on the distribution (temporal and spatial) of K2002 is not
16 sufficient to reproduce the latitudinal gradient of OCS: the seasonal cycles of the fluxes also need
17 to be reconsidered. In this work, the ocean emissions were only modified at certain latitudes by a
18 single regionally-specific factor. Because the role of ocean direct emissions is a subject of debate
19 (Weiss et al., 1995; Xu et al., 2001; Berry et al., 2013; Launois et al., 2015a) and the temporal
20 variations of the direct and indirect ocean emissions are similar (Kettle et al., 2002a), we take all
21 ocean emissions as a whole when rescaling, similarly to the method in Suntharalingam et al.
22 (2008). For all simulations except K2002, a value of 0.5 was applied for the Southern Ocean (30°
23 S - 90° S), while in the tropics (30° N - 30° S), values of 3.2, 5.1, and 5.2 were used for K2002x2,
24 K2002x3, and SiB, respectively, to balance the global budget. Other studies used atmospheric
25 inversions (Berry et al., 2013; Kuai et al., 2015) or an ocean general circulation and
26 biogeochemistry model (Launois et al., 2015a) to access the ocean fluxes, and gain better
27 distribution. The global amount and general latitudinal distribution are consistent with this study.

28 The latitudinal gradient in the boreal region is more sensitive to plant uptake. Increasing plant
29 uptake gives a steeper latitude gradient towards the Arctic. The simulation with K2002x3
30 reproduced the strong gradient in summer and autumn, but the values are lower than the
31 measurements - in agreement with the comparison with FTIR measurements. The mean values of
32 the simulation with K2002x3 at the selected stations are lower than the FTIR measurements.

1 **5.3 Combination of OCS and CO₂ with SiB biospheric fluxes**

2 Although there are still uncertainties in the OCS sources and sinks, apart from land uptake and
3 ocean emissions, their effect on the seasonal cycle in the northern high latitudes is small. Since
4 we only increased the tropical ocean emissions, the ocean effect on the seasonal cycle in the
5 northern high latitudes is smaller than that from land sinks. We used the coupled land fluxes of
6 OCS and CO₂ from SiB to simultaneously simulate OCS and CO₂ with their seasonal cycles
7 connected via the same modeled processes. Through the comparison of both species to the
8 measurements, we can evaluate the GPP and Re in the biosphere model.

9 **5.3.1 OCS simulation with SiB land fluxes**

10 The OCS simulation results with SiB fluxes are shown as magenta triangles in Figure 2. The
11 mean values at the four high/mid latitude sites are higher than those with the original or rescaled
12 K2002 fluxes, especially at Eureka and Ny-Ålesund. The seasonal amplitudes at Eureka, Ny-
13 Ålesund and Bremen are similar to those simulated with K2002x2; and the seasonal amplitude at
14 Jungfraujoch is between those of K2002x2 and K2002x3. From Table 3, shows that the plant
15 uptake of SiB is about three times of K2002, and the soil uptake is also bigger than K2002. With
16 identical distributions of these fluxes, one would expect a similar drawdown during growing
17 season in the Northern Hemisphere from SiB compared to K2002x3. That this is not consistently
18 present at the selected sites indicates that the latitudinal distribution of the land fluxes between
19 SiB and Kettle is different.

20 We compared the difference between SiB and the scaled K2002 plant uptake and soil uptake in
21 July, shown in Figure 4. For the plant uptake, SiB is much smaller than K2002x3 in the boreal
22 forest region, causing a smaller drawdown, while it is stronger in the tropical region. Figure 5
23 (top) shows the monthly plant uptake of different fluxes summed globally, and in three latitude
24 bands: 30°N to 90°N (North); 30°S to 30°N (Equatorial); and 90°S to 30°S (South). In the North
25 region, the total amount and seasonal variation of the SiB plant uptake are similar to K2002x2.
26 The plant uptake of K2002 in the North region accounts for 42% of the global total uptake in a
27 year, while for SiB plant uptake, it contributes only 24%. In Equatorial region the uptake in SiB
28 is much larger than that in K2002x3. In the South, the plant uptake of SiB shows stronger
29 seasonal variation than K2002x3. Globally, the SiB plant uptake is most consistent with K2002x3,
30 though with a smaller seasonality, resulting from the strong uptake in the tropics and Southern

1 Hemisphere. The difference in soil uptake between SiB and K2002 in July shows a similar
2 pattern to the difference in plant uptake: larger uptake in the tropics and smaller uptake in the
3 remaining regions. This latitudinal distribution of SiB OCS land fluxes leads to a higher mean
4 value and smaller seasonal amplitude in the northern high latitudes, as seen from Eureka and Ny-
5 Ålesund. The seasonal amplitude is better represented by SiB at the mid latitude site of
6 Jungfraujoch.

7 Besides the seasonal amplitude, there are phase differences at Bremen and Jungfraujoch between
8 the simulations with SiB fluxes and measurements. Due to the gap during polar winter, these
9 cannot be evaluated at Eureka and Ny-Ålesund. The simulation with SiB shows higher values in
10 the wintertime, which are also seen in the simulations with original and rescaled Kettle's flux.
11 SiB, however, does not have a mechanism for OCS efflux, so the mean overestimation of OCS
12 concentration in winter is by necessity a function of source location/magnitude and/or transport.
13 The simulation with SiB fluxes reaches the minimum earlier than the measurements. If we
14 discount transport errors, this indicates that there is more OCS uptake (either from plants or soils)
15 in the real world than that calculated in the model in the autumn. The minimum offset is not seen
16 in the simulations with K2002x2 and K2002x3, and the seasonal variations of plant uptake are
17 similar in SiB and K2002x2 in the Northern Hemisphere (Figure 5, top), so the early minimum in
18 SiB may result from the smaller soil uptake in autumn compared to K2002, which is shown in
19 Figure 5 (bottom). As mentioned in section 3.3, the soil uptake used in this work is smaller than
20 that in Berry et al. (2013). This could mean that the actual soil uptake is stronger or continues
21 longer. However, the temporal and spatial pattern of K2002 fluxes is with large uncertainties: the
22 plant uptake is estimated from the NPP-base model; the soil uptake is calculated using an
23 empirical algorithm with the parameterization determined for one arable soil type only, which is a
24 likely source of error (Kettle et al., 2002a). Therefore, the early minimum in SiB cannot be
25 attributed to soil uptake through the comparison to K2002. Further investigation is needed to
26 understand the minimum shift.

27 The comparison between the SiB simulation and HIPPO-OCS measurements is shown in
28 magenta lines in Figure 3. The simulation with SiB fluxes results in a lower value in the Southern
29 Hemisphere than the rescaled Kettle fluxes. This matches the HIPPO-OCS better, because SiB
30 has a stronger plant uptake in the tropics and Southern Hemisphere. For the Northern Hemisphere,
31 the low OCS concentrations in the low and mid latitudes (HIPPO-2, HIPPO-3) are due to a

1 combination of sources and/or transport, as are the simulations with Kettle's fluxes. SiB did not
2 capture the strong latitudinal gradient during growing season (HIPPO-5), indicating the plant
3 uptake of OCS in SiB in the boreal forest is too small, at least for the year (2011) in question.

4 **5.3.2 Implications for CO₂ fluxes in SiB from OCS comparison**

5 We hope to gain additional information on the CO₂ biospheric fluxes with the help of OCS. Since
6 the CO₂ and OCS uptake by photosynthesis is coupled in SiB, one can calculate the GPP using
7 the OCS uptake amount. This evaluation is complicated, however, because OCS and CO₂ go
8 through the diffusion and consumption steps independently in SiB. The LRU is a diagnostic
9 quantity that comes out of the simulations following explicit calculation of CO₂ and OCS fluxes.
10 LRU varies by vegetation type, season, and time of day with uncertainties. However, these fluxes
11 can still be evaluated by combining the comparison of OCS and CO₂ between simulations and
12 measurements.

13 As discussed in section 5.3.1, SiB underestimated the OCS drawdown at Eureka and Ny-Ålesund,
14 and poorly represented the latitudinal gradient in the Northern Hemisphere. This indicates that
15 the photosynthetic uptake could be underestimated in northern high latitudes. We examine this
16 further by comparing the CO₂ simulations with measurements.

17 The simulation of CO₂ with SiB fluxes represents the seasonal cycles at all the three sites well
18 (Figure 6, left panels), unlike with the OCS comparison. From the mean seasonal cycles (Figure 6,
19 right panels) the minima in the CO₂ seasonal cycles are later in the simulation than measurements,
20 indicating that the increase of CO₂ after the growing season is slower in the model. We also
21 compared the CO₂ latitudinal distribution between HIPPO-CO₂ and model simulations (Figure 7).
22 The difference in the Southern Hemisphere between the HIPPO-CO₂ and model is very small, so
23 the main disagreement is in the northern high latitudes. In late autumn (HIPPO-2), SiB gives
24 lower values than the HIPPO data in the boreal region. This supports the late minimum in
25 comparison to the FTIR measurements. In spring (HIPPO-3), the simulation is higher than the
26 HIPPO measurements in the Arctic. Previous studies showed that SiB3 performed well in the
27 forest region of North America (Schwalm et al., 2010), while did a poor job in some Arctic
28 tundra regions, caused by an over-sensitivity to very low temperature (Fisher et al., 2014). During
29 the northern growing season, the SiB simulation of CO₂ resulted in a strong latitudinal gradient,
30 which matches the HIPPO measurements well (HIPPO-5), illustrating that the net CO₂ fluxes

1 have a reasonable latitudinal distribution, unlike with the OCS simulation.
2 The seasonal cycle of OCS is mainly influenced by the plant uptake, which is connected with
3 GPP, while CO₂ seasonality results from the sum of both GPP and Re. Huntzinger et al. (2012)
4 have shown that models can get similar NEP with gross fluxes (GPP and Re) that differ by a
5 factor of two or more. If OCS plant uptake is used as a proxy for GPP and the LRU is reasonable,
6 one can infer that the GPP estimated in SiB is low in the northern boreal region, which cannot be
7 seen in the CO₂ simulation driven by NEP, meaning that the Re in SiB must also be low, so that
8 the weak uptake is cancelled out in the net flux. However, the LRU is still uncertain. If LRU is
9 low in general in the Northern Hemisphere, a reasonable GPP estimate could occur together with
10 a small OCS uptake. Therefore the relationship of OCS and CO₂ in SiB needs to be further
11 verified. However, these results indicate that while the NEP is reasonably modeled, its individual
12 component fluxes might be in error. This inference is made possible through the combination of
13 OCS and CO₂ measurements.

14 The early minimum in SiB simulation of OCS compared to the measurements is indicative of
15 weak uptake in the autumn. If this is caused by an weak OCS plant uptake, CO₂ assimilation
16 would also be small, leading to a shorter period of CO₂ drawdown in the simulation, which is the
17 opposite of what is shown in Figure 6. Therefore, it is more likely that OCS soil uptake is too
18 small in SiB in the autumn. Because the OCS soil uptake in SiB is proportional to Rh, the
19 respiration could also be too small. This would explain the late minimum in the CO₂ simulation.
20 Another possibility is that the LRU becomes very large in the autumn, so the OCS uptake is still
21 strong while CO₂ decreases to a very small value. Experiments have shown that the LRU
22 increases under low light condition (Stimler et al., 2010). We do not have sufficient information
23 at this time to determine the most likely reason for SiB to show a shift in the seasonal cycle
24 minimum between the OCS simulation and the measurements. However, the combination of OCS
25 and CO₂ atmospheric measurements opens some new avenues to explore how the biospheric
26 models reproduce the carbon cycle in the real world.

27

28 **6 Conclusions**

29 For the first time, FTIR measurements of OCS and CO₂ were used to study their relationship.
30 OCS retrieved from FTIR spectra at the five sites showed clear seasonal cycles, and confirmed

1 the similarity to CO₂ variations.

2 We compared the OCS column measurements to simulations with original and rescaled versions
3 of fluxes based on Kettle et al. (2002a). The results indicate that increasing the plant uptake and
4 ocean emissions improves the comparison. For the five selected sites in the Northern Hemisphere,
5 increasing plant uptake by a factor of three represented the OCS seasonality well. The OCS
6 simulations were also compared to HIPPO in-situ measurements. Increasing plant uptake leads to
7 a stronger latitudinal gradient in the Northern Hemisphere during growing season and better
8 agreement with HIPPO-OCS. However, the latitudinal distribution of the rescaled fluxes
9 mismatches the HIPPO-OCS measurements in the tropical and northern temperate zone, implying
10 a missing source in that region. Further studies are needed to optimize the OCS sources and sinks.

11 Simulations using coupled SiB land fluxes of CO₂ and OCS show good agreement of CO₂ with
12 FTIR measurements at selected sites, but underestimated OCS drawdown. Through the
13 comparison with HIPPO-OCS measurements, a weaker gradient in the Northern Hemisphere
14 during growing season can be seen in the simulation. Using OCS as a GPP proxy, the GPP
15 estimation in the Northern Hemisphere could be low in SiB. However, the relationship between
16 OCS plant uptake and GPP in the model needs to be further verified.

17 The seasonal cycle minimum offset between simulation and measurements is not consistent for
18 OCS and CO₂. The simulation presents an early minimum for OCS but a late minimum for CO₂
19 when compared to the measurements. These phase differences offer another aspect that can be
20 used to evaluate the photosynthesis and respiration in SiB. Several possibilities which could
21 cause this inconsistency have been discussed, but further research is needed before reaching a
22 conclusion. Looking at OCS and CO₂ together inspires some new thoughts in how the biospheric
23 models reproduce the carbon cycle in the real world.

24

25 **7 Outlook**

26 This work will be extended to more sites, including some in the Southern Hemisphere, to
27 evaluate the seasonal cycles of OCS and CO₂ in different regions. The FTIR networks will
28 provide an additional database for using OCS to constraint GPP, which would be further
29 improved if more frequency, simultaneous measurements of OCS and CO₂ where available at a
30 greater number of sites.

1 Using coupled OCS and CO₂ land fluxes in a biospheric model and comparing to measurements
2 of both gases provides the method to constrain GPP with the help of OCS. The relationship
3 between OCS and CO₂ uptake in SiB can be further verified by field measurements for more
4 plant types and at different time. This will increase the confidence for making conclusions on
5 GPP distribution and time variation from the view of OCS.

6 Although the relationship between OCS plant uptake and GPP still has uncertainties, OCS could
7 be used to study the biospheric processes driving the inter-annual variability. Some climate
8 extremes have impacts on both photosynthesis and respiration; for instance, high temperature
9 could decrease photosynthetic production and increase respiration. With the help of OCS, these
10 biospheric feedbacks could be distinguished.

11

12 **Acknowledgements:**

13 This work is partly supported by the DFG, project PA 1714/6-1. Nicholas Deutscher is supported
14 by an Australian Research Council – Discovery Early Career Researcher Award, DE140100178.
15 We thank the AWI for support in carrying out the measurements in Ny-Ålesund, Spitsbergen.
16 The University of Liège contribution to the present work has primarily been supported by the
17 A3C and ACROSAT PRODEX projects (Belgian Science Policy Office, BELSPO, Brussels).
18 The Liege team further acknowledges crucial support by MeteoSwiss (GAW-CH), the F.R.S. –
19 FNRS and the Fédération Wallonie-Bruxelles. We thank the International Foundation High
20 Altitude Research Stations Jungfrauoch and Gornergrat (HFSJG, Bern). The National Center for
21 Atmospheric Research is supported by the National Science Foundation. The NCAR FTS
22 observation program at Mauna Loa, HI is supported under contract by the National Aeronautics
23 and Space Administration (NASA). We wish to thank NOAA for support of the MLO station.
24 The Eureka measurements were made at the Polar Environment Atmospheric Research
25 Laboratory (PEARL) by the Canadian Network for the Detection of Atmospheric Change
26 (CANDAC), led by James R. Drummond, and in part by the Canadian Arctic ACE Validation
27 Campaigns, led by Kaley A. Walker. They were supported by the AIF/NSRIT, CFI, CFCAS,
28 CSA, EC, GOC-IPY, NSERC, NSTP, OIT, PCSP, and ORF. Additionally, we thank Steve Wofsy
29 and all other HIPPO members for making the HIPPO and NOAA data available to the public
30 from the HIPPO website at <http://hippo.ornl.gov/>.

1

2 **References**

- 3 Adler, A. F., Huffman, G. J., Chang, A., Ferraro, R., Xie, P.-P., Janowiak, J., Rudolf, B.,
4 Schneider, U., Curtis, S., Bolvin, D., Gruber, A., Susskind, J., Arkin, P., and Nelkin, E.: The
5 Version-2 Global Precipitation Climatology Project (GPCP) Monthly Precipitation Analysis
6 (1979–Present), *J. Hydrometeorol.*, 4, 1147–1167, 2003.
- 7 Atkinson, R., Baulch, D. L., Cox, R. A., Hampson Jr., R. F., Kerr, J. A., Rossi, J. M., and Troe J.:
8 Evaluated kinetic, photochemical and heterogeneous data for atmospheric chemistry, *J. Phys.*
9 *Chem. Ref. Data*, 26, 521-1011, 1997.
- 10 Badger, M. R., and Price G. D.: The role of carbonic-anhydrase in photosynthesis, *Annu. Rev.*
11 *Plant Phys.*, 45, 369-392, 1994.
- 12 Baker, D. F., Law, R. M., Gurney, K. R., Rayner, P., Peylin, P., Denning, A. S., Bousquet, P.,
13 Bruhwiler, L., Chen, Y.-H., Ciais, P., Fung, I. Y., Heimann, M., John, J., Maki, T., Maksyutov, S.,
14 Masarie, K., Prather, M., Pak, B., Taguchi, S., and Zhu, Z.: TransCom 3 inversion
15 intercomparison: Impact of transport model errors on the interannual variability of regional CO₂
16 fluxes, 1988–2003, *Global Biogeochem. Cy.*, 20, GB1002, doi:10.1029/2004GB002439, 2006.
- 17 Baker, I. T., Harper, A. B., da Rocha, H. R., Denning, A. S., Araújo, A. C., Borma, L. S., Freitas,
18 H. C., Goulden, M. L., Manzi, A. O., Miller, S. D., Nobre, A. D., Restrepo-Coupe, N., Saleska, S.
19 R., Stöckli, R., von Randow, C., and Wofsy, S. C.: Surface ecophysiological behavior across
20 vegetation and moisture gradients in tropical South America, *Agr. Forest Meteorol.*, 182, 177-188,
21 doi:10.1016/j.agrformet.2012.11.015, 2013.
- 22 Barkley, M. P., Palmer, P. I., Boone, C. D., Bernath, P. F., and Suntharalingam, P.: Global
23 distributions of carbonyl sulfide in the upper troposphere and stratosphere, *Geophys. Res.*
24 *Lett.*, 35, L14810, doi:10.1029/2008GL034270, 2008. Barthlott, S., Schneider, M., Hase, F.,
25 Wiegele, A., Christner, E., Gonzalez, Y., Blumenstock, T., Dohe, S., Garcia, O., Sepúlveda, E.,
26 Strong, K., Mendonca, J., Weaver, D., Palm, M., Deutscher, N. M., Warneke, T., Notholt, J.,
27 Lejeune, B., Mahieu, E., Jones, N., Griffith, D. W. T., Velasco, V. A., Smale, D., Rohbinson, J.,
28 Kivi, R., Heikkinen, P., and Raffalski, U.: Using XCO₂ retrievals for assessing the long-term
29 consistency of NDACC/FTIR data sets, *Atmos. Meas. Tech.*, 8, 1555-1573, doi:10.5194/amt-8-
30 1555-2015, 2015.

1 Beer, C., Reichstein, M., Tomelleri, E., Ciais, P., Jung, M., Carvalhais, N., Rödenbeck, C., Arain,
2 M. A., Baldocchi, D., Bonan, G. B., Bondeau, A., Cescatti, A., Lasslop, G., Lindroth, A., Lomas,
3 M., Luyssaert, S., Margolis, H., Oleson, K. W., Rouspard, O., Veenendaal, E., Viovy, N.,
4 Williams, C., Woodward, F. I., and Papale, D.: Terrestrial gross carbon dioxide uptake: Global
5 Distribution and covariation with climate, *Science*, 329, 834-838, doi:10.1126/science.1184984,
6 2010.

7 Belviso, S., Schmidt, M., Yver, C., Ramonet, M., Gros, V., and Launois, T.: Strong similarities
8 between nighttime deposition velocities of carbonyl sulphide and molecular hydrogen inferred
9 from semi-continuous atmospheric observations in Gif-sur-Yvette, Paris region, *Tellus B*, 65,
10 20719, doi:10.3402/tellusb.v65i0.20719, 2013.

11 Berkelhammer, M., Asaf, D., Still, C., Montzka, S., Noone, D., Gupta, M., Provencal, R., Chen,
12 H., and Yakir, D.: Constraining surface carbon fluxes using in situ measurements of carbonyl
13 sulfide and carbon dioxide, *Global Biogeochem. Cy.*, 28, 161-179, doi:10.1002/2013GB004644,
14 2014.

15 Berry, J., Wolf, A., Campbell, J. E., Baker, I., Blake, N., Blake, D., Denning, A. S., Kawa, S. R.,
16 Montzka, S. A., Seibt, U., Stimler, K., Yakir, D., and Zhu, Z.: A coupled model of the global
17 cycles of carbonyl sulfide and CO₂: a possible new window on the carbon cycle, *J. Geophys.*
18 *Res.-Biogeo.*, 118, 842-852, 2013.

19 Bey, I., Jacob, D. J., Yantosca, R. M., Logan, J. A., Field, B. D., Fiore, A. M., Li, Q., Liu, H. Y.,
20 Mickley, L. J., and Schultz, M. G.: Global modeling of tropospheric chemistry with assimilated
21 meteorology: Model description and evaluation, *J. Geophys. Res.-Atmos.*, 106, 23073-23095,
22 doi:10.1029/2001JD000807, 2001.

23 Buschmann, M., Deutscher, N. M., Sherlock, V., Palm, M., Warneke, T., and Notholt, J.:
24 Retrieval of xCO₂ from ground-based mid-infrared (NDACC) solar absorption spectra and
25 comparison to TCCON, *Atmos. Meas. Tech.*, in review, 2015.

26 Campbell, J. E., Carmichael, G. R., Chai, T., Mena-Carrasco, M., Tang, Y., Blake, D. R., Vay, S.
27 A., Collatz, G. J., Baker, I., Berry, J. A., Montzka, S. A., Sweney, C., Schnoor, J. L., and Stanier,
28 C. O.: Photosynthetic control of atmospheric carbonyl sulfide during the growing season, *Science*,
29 322, 1085-1088, 2008.

30 Campbell, J. E., Whelan, M. E., Seibt, U., Smith, S. J., Berry, J. A., and Hilton, T. W.:

1 Atmospheric carbonyl sulfide sources from anthropogenic activity: Implications for carbon cycle
2 constraints, *Geophys. Res. Lett.*, 42, 3004-3010, 2015.

3 Cheng, Y., Zhang, C., Zhang, Y., Zhang, H., Sun, X., and Mu, Y.: Characteristics and
4 anthropogenic sources of carbonyl sulfide in Beijing, *J. Environ. Sci.*, 28, 163-170,
5 doi:10.1016/j.jes.2014.05.052, 2015.

6 Chin, M., and Davis, D. D.: A reanalysis of carbonyl sulfide as a source of stratospheric
7 background sulfur aerosol. *J. Geophys. Res.*, 100(D5):8993–9005, 1995.

8 Corbin, K. D., Denning, A. S., Lu, L., Wang, J.-W., and Baker, I. T.: Possible representation
9 errors in inversions of satellite CO₂ retrievals, *J. Geophys. Res.*, 113, D2,
10 doi:10.1029/2007JD008716, 2008.

11 Denning, A. S., Collatz, G. J., Zhang, C., Randall, D. A., Berry, J. A., Sellers, P. J., Colello, G.
12 D., and Dazlich, D. A.: Simulation of terrestrial carbon metabolism and atmospheric CO₂ in a
13 general circulation model. Part I: Surface carbon fluxes, *Tellus B*, 48, 521-542, 1996.

14 Denning, A. S., Nicholls, M., Prihodko, L., Baker, I., Vidale, P.-L., Davis, K., and Bakwin, P.:
15 Simulated variations in atmospheric CO₂ over a Wisconsin forest using a coupled ecosystem–
16 atmosphere model, *Glob. Change Biol.*, 9, 1241-1250, 2003.

17 Evans, J. R., Caemmerer, S. V., Setchell, B. A., and Hudson, G. S.: The relationship between
18 CO₂ transfer conductance and leaf anatomy in transgenic tobacco with a reduced content of
19 Rubisco, *Aust. J. Plant Physiol.*, 21, 475-495, 1994.

20 Fisher, J. B., Sikka, M., Oechel, W. C., Huntzinger, D. N., Melton, J. R., Koven, C. D., Ahlström,
21 A., Arain, M. A., Baker, I., Chen, J. M., Ciais, P., Davidson, C., Dietze, M., El-Masri, B., Hayes,
22 D., Huntingford, C., Jain, A. K., Levy, P. E., Lomas, M. R., Poulter, B., Price, D., Sahoo, A. K.,
23 Schaefer, K., Tian, H., Tomelleri, E., Verbeeck, H., Viovy, N., Wania, R., Zeng, N., and Miller,
24 C. E.: Carbon cycle uncertainty in the Alaskan Arctic, *Biogeosciences*, 11, 4271-4288,
25 doi:10.5194/bg-11-4271-2014, 2014.

26 Glatthor, N., Höpfner, M., Baker, I. T., Berry, J., Campbell, J. E., Kawa, S. R., Krysztofiak, G.,
27 Leyser, A., Sinnhuber B.-M., and Stinecipher, J.: Tropical sources and sinks of carbonyl sulfide
28 observed from space, *Geophys. Res. Lett.*, 42, 10082-10090, doi: 10.1002/2015GL066293,
29 2015.Goldan, P. D., Fall, R., Kuster, W. C., and Fehsenfeld, F. C.: Uptake of cos by growing
30 vegetation: A major tropospheric sink, *J. Geophys. Res.*, 93, D11, 14186-14192, 1988.

1 Guo, H., Simpson, I. J., Ding, A. J., Wang, T., Saunders, S. M., Wang, T. J., Cheng, H. R.,
2 Barletta, B., Meinardi, S., Blake, D. R., and Rowland, F. S.: Carbonyl sulfide, dimethyl sulfide
3 and carbon disulfide in the Pearl River Delta of southern China: Impact of anthropogenic and
4 biogenic sources. *Atmos. Environ.*, 44, 31, 3805-3813, doi:10.1016/j.atmosenv.2010.06.040,
5 2010. Huntzinger, D., Post, W., Michelak, A., Wei, Y., Jacobsen, A., West, T. O., Baker, I., Chen,
6 J., Davis, K., Hayes, D., Hoffman, F., Jain, A., Liu, S., McGuire, D., Neilson, R., Poulter, B.,
7 Tian, H., Thornton, P., Tomelleri, E., Viovy, N., Xiao, J., Zeng, N., Zhao, M., and Cook, R.:
8 North American Carbon Project (NACP) regional interim synthesis: terrestrial biospheric model
9 intercomparison, *Ecol. Model.*, 232, 144-157, doi:10.1016/j.ecolmodel.2012.02.004, 2012.

10 Jung, M., Reichstein, M., Margolis, H. A., Cescatti, A., Richardson, A. D., Arain, M. A., Arneeth,
11 A., Bernhofer, C., Bonal, D., Chen, J., Gianelle, D., Gobron, N., Kiely, G., Kutsch, W., Lasslop,
12 G., Law, B. E., Lindroth, A., Merbold, L., Montagnani, L., Moors, E. J., Papale, D., Sottocornola,
13 M., Vaccari, F., and Williams, C.: Global patterns of land-atmosphere fluxes of carbon dioxide,
14 latent heat, and sensible heat derived from eddy covariance, satellite, and meteorological
15 observations, *J. Geophys. Res.*, 116, G00J07, doi:10.1029/2010JG001566, 2011.

16 Keppel-Aleks, G., Wennberg, P. O., and Schneider, T.: Sources of variations in total column
17 carbon dioxide, *Atmos. Chem. Phys.*, 11, 3581-3593, doi:10.5194/acp-11-3581-2011, 2011.

18 Kettle, A. J., Kuhn, U., von Hobe, M., Kesselmeier, J., and Andreae, M. O.: Global budget of
19 atmospheric carbonyl sulfide: temporal and spatial variations of the dominant sources and sinks, *J.*
20 *Geophys. Res.-Atmos.*, 107, 4658, doi:10.1029/2002JD002187, 2002a.

21 Kettle, A. J., Kuhn, U., von Hobe, M., Kesselmeier, J., Liss, P. S., and Andreae, M. O.: Comparin
22 g forward and inverse models to estimate the seasonal variation of hemisphere-intergrated fluxes
23 of carbonyl sulfide, *Atmos. Chem. Phys.*, 2, 343-361, 2002b.

24 Kuai, L., Worden, J., Kulawik, S. S., Montzka, S. A., and Liu, J.: Characterization of aura
25 tropospheric emissions spectrometer carbonyl sulfide retrievals over ocean, *Atmos. Meas. Tech.*,
26 7, 163-172, doi:10.5194/amt-7-163-2014, 2014.

27 Kuai, L., Worden, J. R., Campbell, J. E., Kulawik, S. S., Lee, M., Weidner, R. J., Li, K., Montzka,
28 S. A., Moore, F. L., Berry, J. A., Baker, I., Denning, S., Bian, H., Bowman, K., Liu, J., and Yung,
29 Y.: Estimate of Carbonyl Sulfide Tropical Oceanic Surface Fluxes Using Aura Tropospheric
30 Emission Spectrometer Observations, *J. Geophys. Res.-Atmos.*, accepted,

1 doi:10.1002/2015JD023493, 2015.

2 Launois, T., Belviso, S., Bopp, L., Fichot, C. G., and Peylin, P.: A new model for the global
3 biogeochemical cycle of carbonyl sulfide – Part 1: Assessment of direct marine emissions with an
4 oceanic general circulation and biogeochemistry model, *Atmos. Chem. Phys.*, 15, 2295-2312,
5 2015a.

6 Launois, T., Peylin, P., Belviso, S., and Poulter, B.: A new model of the global biogeochemical
7 cycle of carbonyl sulfide – Part 2: Use of carbonyl sulfide to constrain gross primary productivity
8 in current vegetation models, *Atmos. Chem. Phys.*, 15, 9285-9312, doi:10.5194/acp-15-9285-
9 2015, 2015. Montzka, S. A., Calvert, P., Hall, B. D., Elkins, J. W., Conway, T. J., Tans, P. P., and
10 Sweeney, C.: On the global distribution, seasonality, and budget of atmospheric carbonyl sulfide
11 (COS) and some similarities to CO₂, *J. Geophys. Res.-Atmos.*, 112, D09302,
12 doi:10.1029/2006JD007665, 2007.

13 Nassar, R., Jones, D. B. A., Suntharalingam, P., Chen, J. M., Andres, R. J., Wecht, K. J.,
14 Yantosca, R. M., Kulawik, S. S., Bowman, K. W., Worden, J. R., Machida T., and Matsueda H.:
15 Modeling global atmospheric CO₂ with improved emission inventories and CO₂ production from
16 the oxidation of other carbon species, *Geoscientific Model Development*, 3, 689-716, 2010.

17 Nguyen, B. C., Mihalopoulos, N., Putaud, J. P., and Bonsang, B.: Carbonyl sulfide emissions
18 from biomass burning in the tropics, *J. Atmos. Chem.*, 22, 55-65, 1995.

19 Nicholls, M. E., Denning, A. S., Prihodko, L., Vidale, P.-L., Baker, I., Davis, K., and Bakwin, P.:
20 A multiple-scale simulation of variations in atmospheric carbon dioxide using a coupled
21 biosphere–atmosphere model, *J. Geophys. Res.*, 109, D18, doi:10.1029/2003JD004482, 2004.

22 Notholt, J., Kuang, Z., Rinsland, C. P., Toon, G. C., Rex, M., Jones, N., Albrecht, T.,
23 Deckelmann, H., Krieg, J., Weinzierl, C., Bingemer, H., Weller, R., and Schrems, O.: Enhanced
24 upper tropical tropospheric COS: Impact on the stratospheric aerosol layer, *Science*, 300, 5617,
25 307-310, doi: 10.1126/science.1080320, 2003. Olsen, S. C., and Randerson, J. T.: Differences
26 between surface and column atmospheric CO₂ and implications for carbon cycle research, *J.*
27 *Geophys. Res.*, 109, D02301, doi:10.1029/2003JD003968, 2004.

28 Park, R. J., Jacob, D. J., Field, B. D., Yantosca, R. M., and Chin, M.: Natural and transboundary
29 pollution influences on sulfate-nitrate-ammonium aerosols in the United States: Implications for
30 policy, *J. Geophys. Res.*, 109, D15204, doi:10.1029/2003JD004473, 2004.

1 Protoschill-Krebs, G. and Kesselmeier, J.: Enzymatic pathways for the consumption of carbonyl
2 sulphide (COS) by higher plants, *Bot. Acta*, 105, 206–212, doi:10.1111/j.1438-
3 8677.1992.tb00288.x, 1992.

4 Protoschill-Krebs, G., Wilhelm, C., and Kesselmeier, J.: Consumption of carbonyl sulphide (COS)
5 by higher plant carbonic anhydrase (CA), *Atmos. Environ.*, 30, 18, 3151–3156,
6 doi:10.1016/1352-2310(96)00026-X, 1996. Raich, J. W., Rastetter, E. B., Melillo, J. M.,
7 Kicklighter, D. W., Steudler, P. A., Peterson, B. J., Grace, A. L., Moore III, B., and Vorosmarty,
8 C. J.: Potential Net Primary Productivity in South America: Application of a Global Model, *Ecol.*
9 *Appl.*, 1, 399-429, 1991.

10 Randall, D. A., Dazlich, D. A., Zhang, C., Denning, A. S., Sellers, P. J., Tucker, C. J., Bounoua,
11 L., Berry, J. A., Collatz, G. J., Field, C. B., Los, S. O., Justice, C. O., and Fung, I.: A revised land
12 surface parameterization (SiB2) for GCMs. Part III: the greening of the Colorado State
13 University General Circulation Model, *J. Climate*, 9, 738-763, 1996.

14 Rienecker, M. M., Suarez, M. J., Gelaro, R., Todling, R., Bacmeister, J., Liu, E., Bosilovich, M.
15 G., Schubert, S. D., Takacs, L., Kim, G.-K., Bloom, S., Chen, J., Collins, D., Conaty, A., da Silva,
16 A., Gu, W., Joiner, J., Koster, R. D., Lucchesi, R., Molod, A., Owens, T., Pawson, S., Pegion, P.,
17 Redder, C. R., Reichle, R., Robertson, F. R., Ruddick, A. G., Sienkiewicz, M., and Woollen, J.:
18 MERRA: NASA's Modern-Era Retrospective Analysis for Research and Applications, *J.*
19 *Climate*, 24, 3624–3648, 2011.

20 Rodgers, C. D., *Inverse Methods for Atmospheric Sounding: Theory and Practice*, Series
21 *Atmospheric, Oceanic and Planetary Physics*, vol.2, 238pp., World Scientific, Singapore, 2000.

22 Rodgers, C. D. and Connor, B. J.: Intercomparison of remote sounding instruments, *J. Geophys.*
23 *Res.*, 108, 4116, doi:10.1029/2002JD002299, 2003.

24 Sandoval-Soto, L., Stanimirov, M., von Hobe, M., Schmitt, V., Valdes, J., Wild, A., and
25 Kesselmeier, J.: Global uptake of carbonyl sulfide (COS) by terrestrial vegetation: Estimates
26 corrected by deposition velocities normalized to the uptake of carbon dioxide (CO₂),
27 *Biogeosciences*, 2, 125-132, doi:10.5194/bg-2-125-2005, 2005.

28 Sato, N., Sellers, P. J., Randall, D. A., Schneider, E. K., Shukla, J., Kinter, J. L., Hou, Y-T., and
29 Albertazzi, E.: Effects of implementing the Simple Biosphere Model in a General Circulation
30 Model, *J. Atmos. Sci.*, 46, 2757-2782, 1989.

1 Schwalm, C. R., Williams, C. A., Schaefer, K., Anderson, R., Arain, M. A., Baker, I., Barr, A.,
2 Black, T. A., Chen, G. S., Chen, J. M., Ciais, P., Davis, K. J., Desai, A., Dietze, M., Dragoni, D.,
3 Fischer, M. L., Flanagan, L. B., Grant, R., Gu, L. H., Hollinger, D., Izaurralde, R. C., Kucharik,
4 C., Lafleur, P., Law, B. E., Li, L. H., Li, Z. P., Liu, S. G., Lokupitiya, E., Luo, Y. Q., Ma, S. Y.,
5 Margolis, H., Matamala, R., McCaughey, H., Monson, R. K., Oechel, W. C., Peng, C. H., Poulter,
6 B., Price, D. T., Riciutto, D. M., Riley, W., Sahoo, A. K., Sprintsin, M., Sun, J. F., Tian, H. Q.,
7 Tonitto, C., Verbeeck, H., and Verma, S. B.: A model-data intercomparison of CO₂ exchange
8 across North America: Results from the North American Carbon Program site synthesis, *J.*
9 *Geophys. Res.-Biogeo.*, 115, G00H05, doi:10.1029/2009JG001229, 2010.

10 Sellers, P. J., Mintz, Y., Sud, Y. C., and Dalcher A.: A simple biosphere model (SIB) for use
11 within general-circulation models, *J. Atmos. Sci.*, 43, 505-531, 1986.

12 Seibt, U., Kesselmeier, J., Sandoval-Soto, L., Kuhn, U., and Berry, J. A.: A kinetic analysis of
13 leaf uptake of COS and its relation to transpiration, photosynthesis and carbon isotope
14 fractionation, *Biogeosciences*, 7, 333-341, doi:10.5194/bg-7-333-2010, 2010.

15 Steinbacher, M., Bingemer, H. G., and Schmidt, U.: Measurements of the exchange of carbonyl
16 sulfide (OCS) and carbon disulfide (CS₂) between soil and atmosphere in a spruce forest in
17 central Germany. *Atmos. Environ.*, 38, 35, 6043-6052, doi:10.1016/j.atmosenv.2004.06.022,
18 2004.Stimler, K., Montzka, S. A., Berry, J. A., Rudich, Y., and Yakir, D.: Relationships between
19 carbonyl sulfide (COS) and CO₂ during leaf gas exchange, *New Phytol.*, 186, 869-878, 2010.

20 Stimler, K., Berry, J. A., and Yakir, D.: Effects of carbonyl sulfide and carbonic anhydrase on
21 stomatal conductance, *Plant Physiol.*, 158, 524-530, 2012.

22 Stöckli, R., Rutishauser, T., Dragoni, D., O'Keefe, J., Thornton, P. E., Jolly, M., Lu, L., Denning,
23 A. S.: Remote sensing data assimilation for a prognostic phenology model, *J. Geophys. Res.-*
24 *Biogeo.*, 113, G04021, doi:10.1029/2008JG000781, 2008.

25 Stöckli, R., Rutishauser, T., Baker, I., Körner, C., Liniger, M. A., and Denning, A. S.: A Global
26 Reanalysis of Vegetation Phenology, *J. Geophys. Res.-Biogeo.*, 116, G03020,
27 doi:10.1029/2010JG001545, 2011.

28 Sun, W., Maseyk, K., Lett, C., and Seibt, U.: A soil diffusion–reaction model for surface COS
29 flux: COSSM v1, *Geosci. Model Dev.*, 8, 3055-3070, doi:10.5194/gmd-8-3055-2015,
30 2015.Suntharalingam, P., Spivakovsky, C. M., Logan, J. A., and McElroy, M. B.: Estimating the

1 distribution of terrestrial CO₂ sources and sinks from atmospheric measurements: Sensitivity to
2 configuration of the observation network, *J. Geophys. Res.*, 108, 4452,
3 doi:10.1029/2002JD002207, 2003.

4 Suntharalingam, P., Jacob, D. J., Palmer, P. I., Logan, J. A., Yantosca, R. M., Xiao, Y., Evans, M.
5 J., Streets, D. G., Vay, S. L., and Sachse, G. W.: Improved quantification of Chinese carbon
6 fluxes using CO₂/CO correlations in Asian outflow, *J. Geophys. Res.*, 109, D18S18,
7 doi:10.1029/2003JD004362, 2004.

8 Suntharalingam, P., Kettle, A. J., Montzka, S. M., and Jacob, D. J.: Global 3-D model analysis of
9 the seasonal cycle of atmospheric carbonyl sulfide: implications for terrestrial vegetation uptake,
10 *Geophys. Res. Lett.*, 35, L19801, doi:10.1029/2008GL034332, 2008.

11 Takahashi, T., Sutherland, S. C., Wanninkhof, R., Sweeney, C., Feely, R. A., Chipman, D. W.,
12 Hales, B., Friederich, G., Chavez, F., Sabine, C., Watson, A., Bakker, D. C. E., Schuster, U.,
13 Metzl, N., Yoshikawa-Inoue, H., Ishii, M., Midorikawa, T., Nojiri, Y., Körtzinger, A., Steinhoff,
14 T., Hoppema, M., Olafsson, J., Arnarson, T. S., Tilbrook, B., Johannessen, T., Olsen, A.,
15 Bellerby, R., Wong, C. S., Delille, B., Bates, N. R., and de Baar, H. J. W.: Climatological mean
16 and decadal change in surface ocean pCO₂, and net sea-air CO₂ flux over the global oceans,
17 *Deep Sea Research Part II: Topical Studies in Oceanography*, 56, 554-577,
18 doi:10.1016/j.dsr2.2008.12.009, 2009.

19 Van Diest, H., and Kesselmeier J.: Soil atmosphere exchange of carbonyl sulfide (COS) regulated
20 by diffusivity depending on water-filled pore space, *Biogeosciences*, 5, 475-483, 2008.

21 Wang, J. W., Denning, A. S., Lu, L., Baker, I. T., Corbin, K. D., and Davis, K. J.: Observations
22 and simulations of synoptic, regional, and local variations in atmospheric CO₂, *J. Geophys. Res.*,
23 112, D0418, doi:10.1029/2006JD007410, 2007.

24 Weiss, P. S., Johnson, J. E., Gammon, R. H., and Bates, T. S.: Reevaluation of the open ocean
25 source of carbonyl sulfide to the atmosphere, *J. Geophys. Res.-Atmos*, 100, D11, 23083-23092,
26 doi:10.1029/95JD01926, 1995. Whelan, M. E., Min, D. H., and Rhew, R. C.: Salt marsh
27 vegetation as a carbonyl sulfide (COS) source to the atmosphere, *Atmos. Environ.*, 73, 131-137,
28 2013.

29 Wofsy, S. C., Daube, B. C., Jimenez, R., Kort, E., Pittman, J. V., Park, S., Commane, R., Xiang,
30 B., Santoni, G., Jacob, D., Fisher, J., Pickett-Heaps, C., Wang, H., Wecht, K., Wang, Q.-Q.,

1 Stephens, B. B., Shertz, S., Watt, A. S. , Romashkin, P., Campos, T., Haggerty, J., Cooper, W. A.,
2 Rogers, D., Beaton, S., Hendershot, R., Elkins, J. W., Fahey, D. W., Gao, R. S., Moore, F.,
3 Montzka, S. A., Schwarz, J. P., Perring, A. E., Hurst, D., Miller, B. R., Sweeney, C., Oltmans, S.,
4 Nance, D., Hints, E., Dutton, G., Watts, L. A., Spackman, J. R., Rosenlof, K. H., Ray, E. A.,
5 Hall, B., Zondlo, M. A., Diao, M., Keeling, R., Bent, J., Atlas, E. L., Lueb, R., and Mahoney, M.
6 J.: HIPPO NOAA Flask Sample GHG, Halocarbon, and Hydrocarbon Data (R_20121129),
7 Carbon Dioxide Information Analysis Center, Oak Ridge National Laboratory, Oak Ridge,
8 Tennessee, U.S.A. http://dx.doi.org/10.3334/CDIAC/hippo_013 (Release 20121129), 2012.

9 Wunch, D., Toon, G. C., Wennberg, P. O., Wofsy, S. C., Stephens, B. B., Fischer, M. L., Uchino,
10 O., Abshire, J. B., Bernath, P., Biraud, S. C., Blavier, J.-F. L., Boone, C., Bowman, K. P.,
11 Browell, E. V., Campos, T., Connor, B. J., Daube, B. C., Deutscher, N. M., Diao, M., Elkins, J.
12 W., Gerbig, C., Gottlieb, E., Griffith, D. W. T., Hurst, D. F., Jiménez, R., Keppel-Aleks, G., Kort,
13 E. A., Macatangay, R., Machida, T., Matsueda, H., Moore, F., Morino, I., Park, S., Robinson, J.,
14 Roehl, C. M., Sawa, Y., Sherlock, V., Sweeney, C., Tanaka, T., and Zondlo, M. A.: Calibration
15 of the Total Carbon Column Observing Network using aircraft profile data, *Atmos. Meas. Tech.*,
16 3, 1351-1362, doi:10.5194/amt3-1351-2010, 2010.

17 Wunch, D., Toon, G. C., Blavier, J.-F. L., Washenfelder, R. A., Notholt, J., Connor, B. J., Griffith,
18 D. W. T., Sherlock, V., and Wennberg, P. O.: The Total Carbon Column Observing Network,
19 *Philos. T. R. Soc. A*, 369, 2087-2112, doi:10.1098/rsta.2010.0240, 2011.

20 Xu, X., Bingemer, H. G., Georgii, H.W., Schmidt, U., and Bartell, U.: Measurements of carbonyl
21 sulfide (COS) in surface seawater and marine air, and estimates of the air-sea flux from
22 observations during two Atlantic cruises, *J. Geophys. Res.-Atmos.*, 106, D4, 3491–3502,
23 doi:10.1029/2000JD900571, 2001.

24 Xu, X., Bingemer, H. G., and Schmidt, U.: The flux of carbonyl sulfide and carbon disulfide
25 between the atmosphere and a spruce forest, *Atmos. Chem. Phys.*, 2, 171-181, doi:10.5194/acp-2-
26 171-2002, 2002. Yang, Z., Washenfelder, R. A., Keppel-Aleks, G., Krakauer, N. Y., Randerson, J.
27 T., Tans, P. P., Sweeney, C., and Wennberg, P. O.: New constraints on Northern Hemisphere
28 growing season net flux, *Geophys. Res. Lett.*, 34, L12807, doi:10.1029/2007GL029742, 2007.

29 Yevich, R., and Logan, J. A.: An assessment of biofuel use and burning of agricultural waste in
30 the developing world, *Global Biogeochem. Cy.*, 17, 1095, doi:10.1029/2002GB001952, 2003.

1 Yi, Z. G., Wang, X. M., Sheng, G. Y., Zhang, D. Q., Zhou, G. Y., and Fu, J. M.: Soil uptake of
2 carbonyl sulfide in subtropical forests with different successional stages in south China, J.
3 Geophys. Res., 112, D08302, doi:10.1029/2006JD008048, 2007.

4
5
6
7
8
9
10
11
12
13
14
15
16
17
18
19
20
21
22
23
24
25

1 Table 1. FTIR sites used in this study

Site	Latitude (°N)	Longitude (°E)	Altitude (m a.s. l.)	Instrument	Measurement years	Network
Eureka	80.1	-86.4	610	Bomem DA8 125HR	1993-2008 2006-present	NDACC& TCCON
Ny-Ålesund	78.9	11.9	21	120HR 120-5HR	1992-2012 2013-present	NDACC& TCCON
Bremen	53.1	8.8	27	120HR 125HR	2002-2003 2004-present	NDACC& TCCON
Jungfrauoch	46.5	8.0	3580	homemade 120HR	1984-2008 1990-present	NDACC
Mauna Loa	19.5	-155.6	3397	Bomem DA8 120M	1991-1995 1995-present	NDACC

2
3
4
5
6
7
8
9
10
11

1 Table 2. Summary of the retrieval parameters for OCS

Retrieval code	Spectroscopy	A priori profiles	OCS	A priori matrix	S _a	Microwindows (cm ⁻¹)	Interfering species	SNR	Pressure, Temperature profiles
SFIT4_v0.9.4	Based on HITRAN 2012	Provided by G. Toon over private communication, modified by tropopause height		In-situ measurement variability below 9 km, ACE-FTS measurement variability above 9 km		2047.78-2048.22 2049.75-2050.12 2051.18-2051.48 2054.33-2054.67	O ₃ , H ₂ O, CO, H ₂ ¹⁸ O, ¹³ CO ₂ , ¹⁸ OCO	300 (pre-fixed)	NCEP

2
3
4
5
6
7
8
9
10
11
12
13
14
15
16
17

1 Table 3. Annual global atmospheric OCS budget (fluxes in Gg S year⁻¹)

	K2002 ^a	K2002x2	K2002x3	SiB
	Mean (Range)	Revisions	Revisions	Revisions
<i>Sources</i>				
Anthropogenic	182 (90-266)			
Ocean	280 (39-520)	516	754	757
Biomass burning	35 (25-38) ^b			
<i>Sinks</i>				
Plant	238 (210-270)	475	713	688
Soil	130 (74-180)			159
Tropospheric OH oxidation	96 (95-98) ^b			
Stratosphere loss	28 ^b			
Net	5	4	4	3

2 ^a Modifications include biomass burning, tropospheric OH oxidation, and stratospheric loss. (see
3 text)

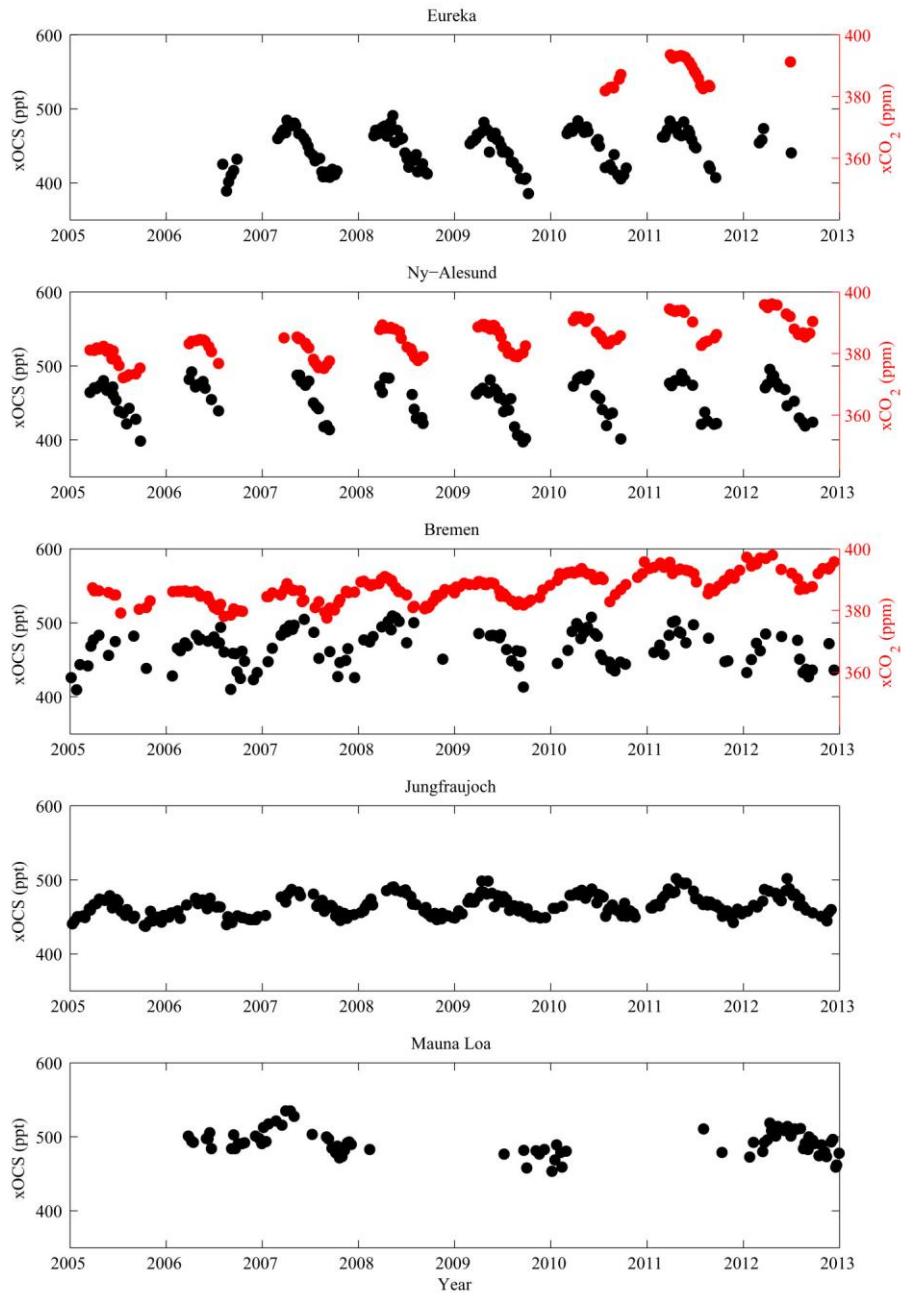
4 ^b The range for biomass burning and tropospheric OH oxidation is the range calculated in the
5 model from 2005 to 2012; the calculated stratospheric loss varies little.

6

7

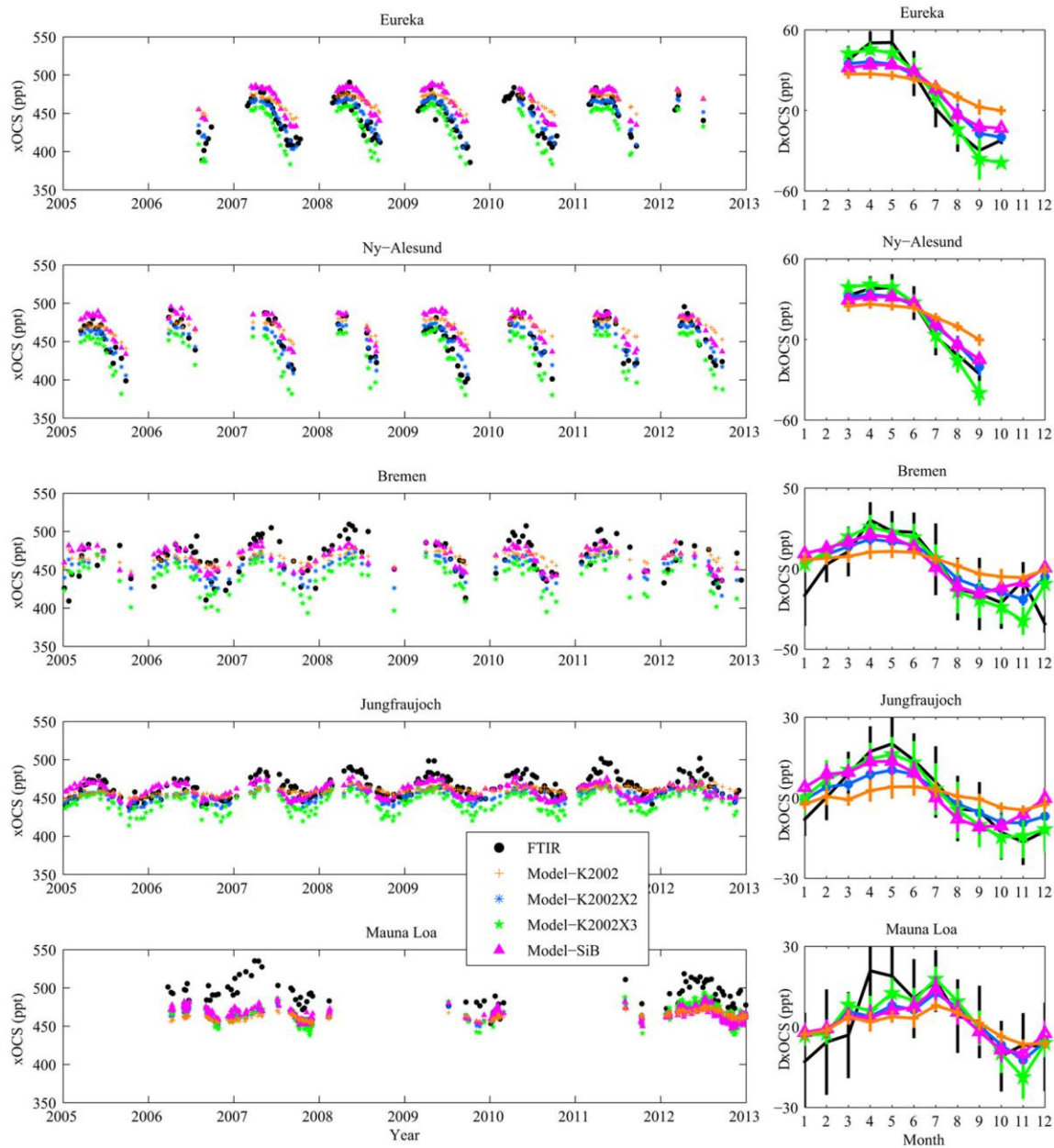
8

9



1
 2 Figure 1. Weekly mean xOCS (black dots) and xCO₂ (red dots) retrieved from FTIR spectra at
 3 Eureka, Ny Ålesund, Bremen, Jungfrauoch and Mauna Loa.

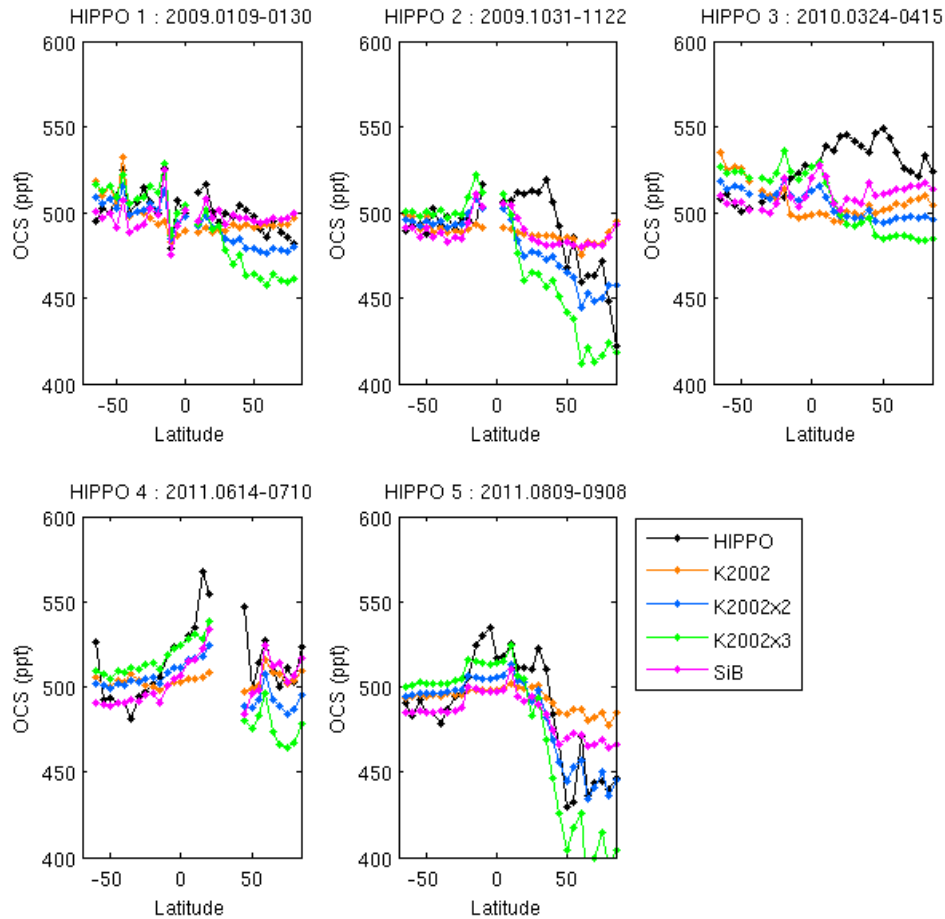
4



1
 2 Figure 2. Comparison of FTIR measurements of OCS to model simulations at Eureka, Ny-
 3 Ålesund, Bremen, Jungfrauoch and Mauna Loa. The left panels show weekly means from 2005
 4 to 2012. The right panels are the monthly mean relative xOCS (relative to annual mean) averaged
 5 for multiple years. The error bars are the standard deviations of each month. The FTIR retrievals
 6 are shown in black dots. The model simulations are driven by K2002 (orange plus signs),
 7 K2002x2 (blue asterisks), K2002x3 (green stars), and SiB (magenta triangles).

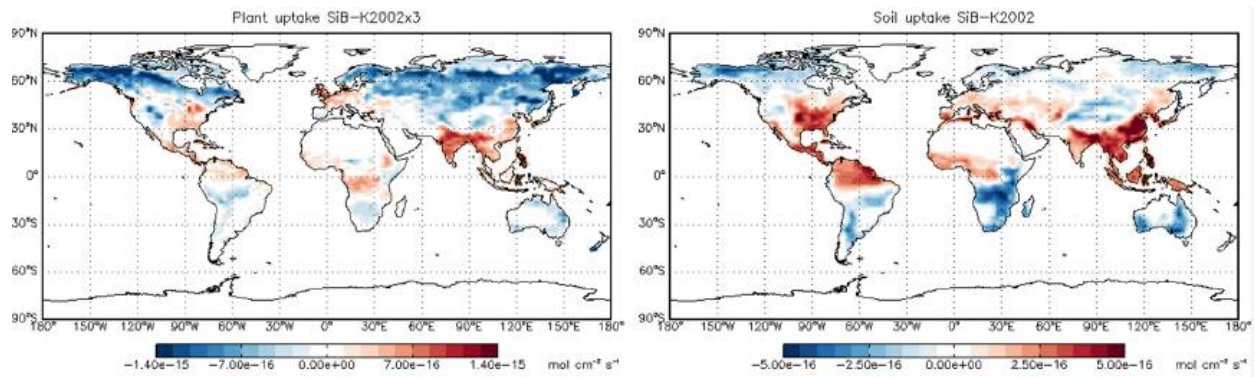
8

9



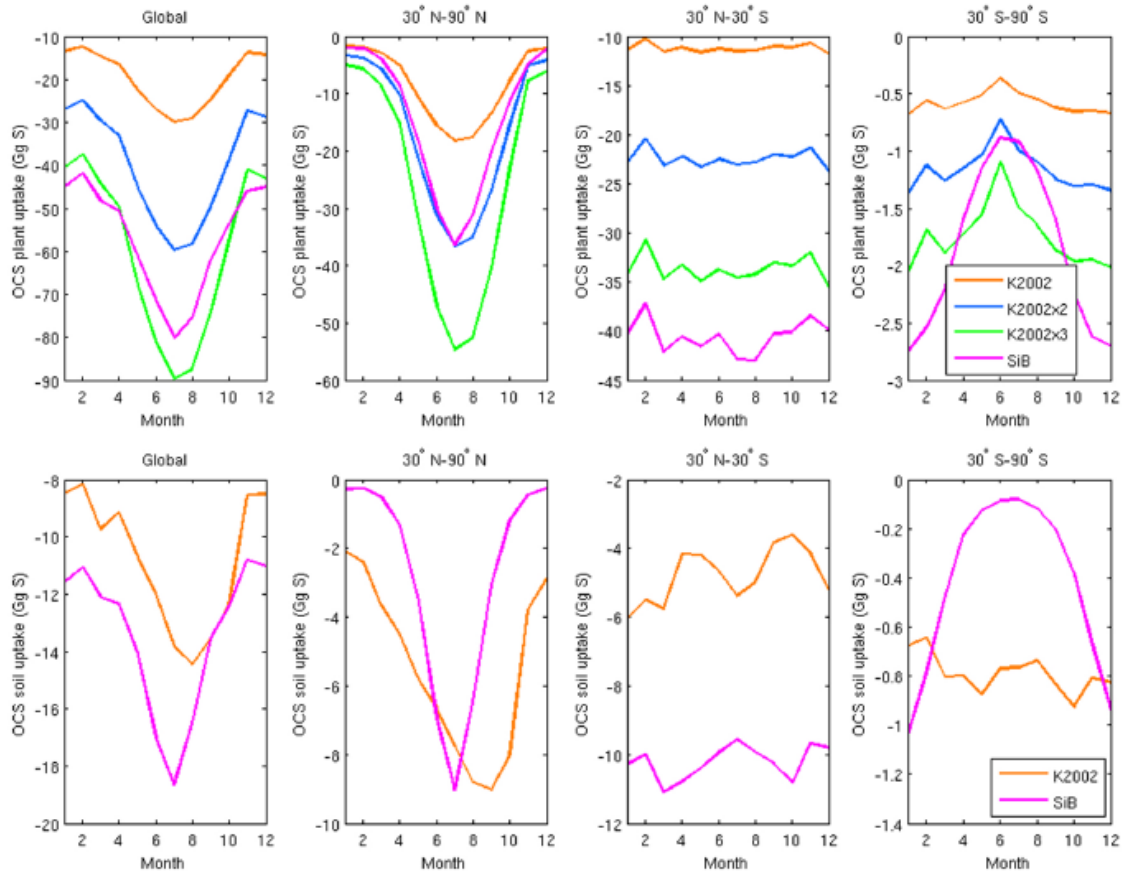
1
2
3
4
5
6
7
8
9
10
11
12
13
14

Figure 3. Comparison of HIPPO OCS measurements and model simulations. The five campaigns are compared separately to show latitudinal gradient at different seasons. To minimize the influence of the stratosphere, only the measurements lower than 9 km are used. The model outputs are selected at the nearest measurement location and time. The measurements and model output are averaged in five degree bins. The HIPPO data are shown in black dots. The model simulations are in the same colors with those shown in Figure 2.



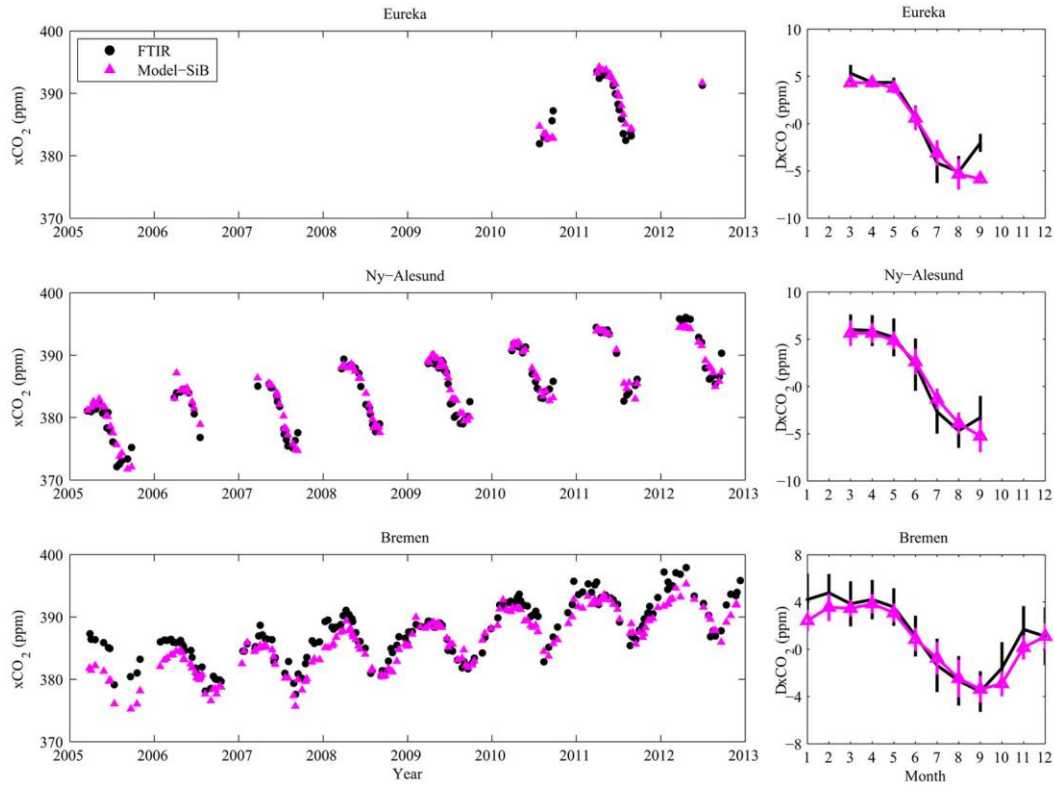
1
2
3
4
5
6
7
8
9
10
11
12
13
14
15
16
17
18
19
20
21

Figure 4. Difference between SiB OCS plant uptake and K2002x3 (left, SiB – K2002x3), difference between OCS soil uptake and K2002 (right, SiB – K2002)



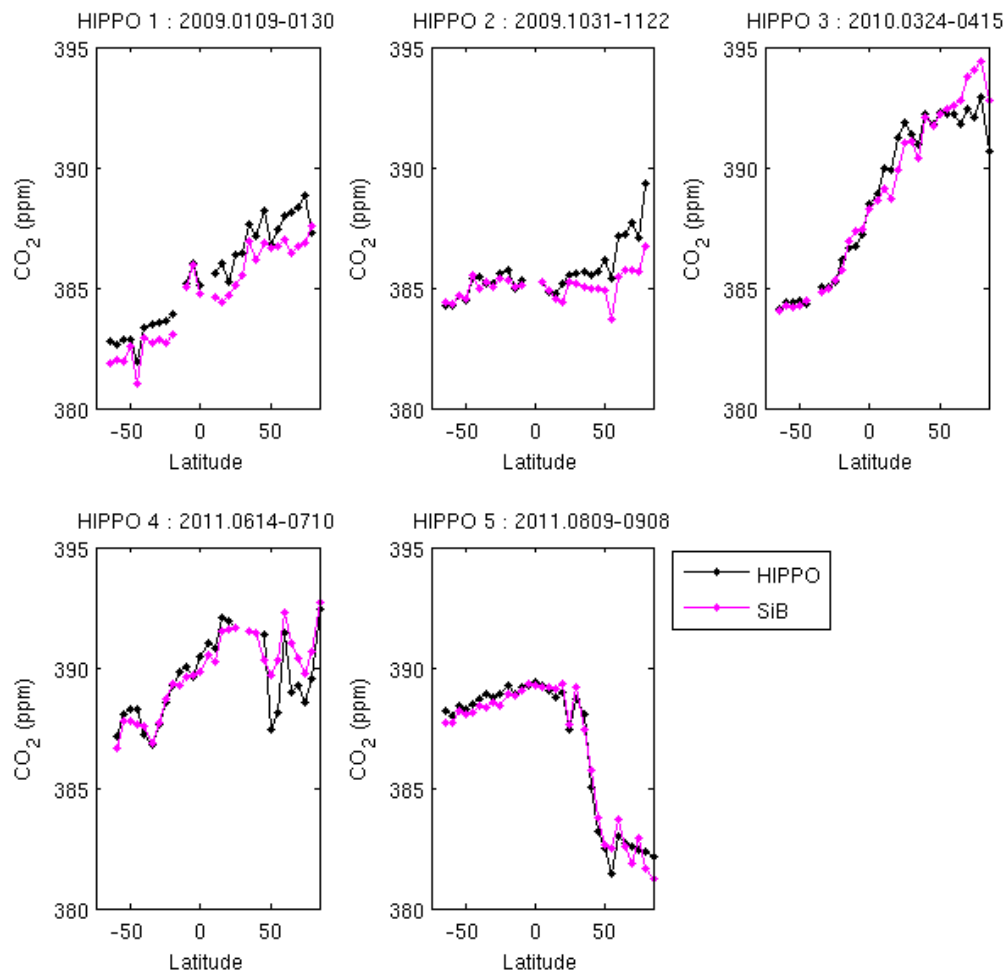
1
2
3
4
5
6
7
8
9
10
11
12
13

Figure 5. Monthly totals of OCS plant uptake (top) and soil uptake (bottom) of K2002 (orange), K2002x2 (blue), K2002x3 (green), and SiB (magenta) for global, 30° N - 90° N, 30°N - 30° S, and 30° S - 90° S.



1
 2 Figure 6. Comparison of FTIR measurements of CO₂ (black dots) to model simulations with SiB
 3 land fluxes (magenta triangles) at Eureka, Ny-Ålesund and Bremen. The left panels show weekly
 4 means from 2005 to 2012. The right panels show the monthly mean relative xCO₂ (relative to
 5 annual mean) averaged for multiple years. The error bars are the standard deviations of each
 6 month.

7
 8
 9
 10
 11
 12
 13
 14
 15



1

2

3

Figure 7. Comparison of HIPPO CO₂ measurements (black) and model simulations with SiB land

4

fluxes (magenta).